NASA CONTRACTOR REPORT

NASA CR-772

NASA CR-772

PLANE-STRESS, ELASTIC-PLASTIC STATES IN THE VICINITY OF CRACK TIPS

by A. S. Kobayashi, S. Woo, and R. C. Shah

Prepared by

UNIVERSITY OF WASHINGTON

Seattle, Wash.

for

NATIONAL AERONAUTICS AND SPACE ADMINISTRATION • WASHINGTON, D. C. • APRIL 1967

NASA CR-772

PLANE-STRESS, ELASTIC-PLASTIC STATES IN THE VICINITY OF CRACK TIPS

By A. S. Kobayashi, S. Woo, and R. C. Shah

Prepared under Grant No. NsG-532 by
UNIVERSITY OF WASHINGTON
Seattle, Wash.

for

NATIONAL AERONAUTICS AND SPACE ADMINISTRATION

For sale by the Clearinghouse for Federal Scientific and Technical Information
Springfield, Virginia 22151 – CFSTI price $3.00

PLANE-STRESS, ELASTIC-PLASTIC STATES IN THE VICINITY OF CRACK TIPS

By A. S. Kobayashi, S. Woo, and R. C. Shah

ABSTRACT

The von Mises yield condition and flow rule are used to analyze the elastic-plastic states in the vicinity of the tip of a straight crack in a thin plate. Elastic-perfectly-plastic material is considered, and the yield zone is assumed to be small in comparison to the crack length.

The numerical method of finite differences is used together with a specially developed iteration operation to solve the nonlinear equations involved. Two cases are analyzed: a plate subjected to uniform in-plane shear and a plate subjected to uniform tension. States of stress in the elastic-plastic regions are determined together with the boundaries of the yield zone.

The numerical results show that stress distributions satisfy the $1/\sqrt{r}$ relation approximately for points away from the crack tip but in the plastic region. These results lend some theoretical support to the plasticity correction factor as utilized in the Griffith-Irwin approach to fracture.

INTRODUCTION

When an infinitely elastic solid with an embedded crack is subjected to a loading condition, the stresses at the crack tip are infinite in magnitude and share a common factor, K, which is referred to as the stress intensity factor. (See, for example, reference 1.) The Griffith-Irwin theory of fracture assumes that this stress intensity factor at the onset of rapid fracture is related to the fracturing force for a brittle material. Experimental evidence indicates that this postulate is correct for many practical problems in engineering.

In a ductile material, however, the stresses at the crack tip are finite in magnitude and the concept of stress intensity factor no longer holds. For such a ductile material, the computed critical fracturing force according to the Griffith-Irwin theory and measured forces are not always in good agreement. In order to compensate for this discrepancy, Irwin suggested that a portion of the width of the plastically yielded region be added to the actual crack length at fracture and that this corrected crack length be used to compute the critical fracturing force (ref. 2). Substantial experimental evidence now exists to show that such corrections could be used to extend the theory of linear fracture mechanics to cover the ductile material. The exact amount of added crack length for such yield correction is a subject of debate. It depends on the state of stresses in the plastically yielded region as well as the surrounding elastic field. In order to determine Irwin's yield correction factor with accuracy, then, it is necessary to know the state of stresses in the vicinity of the crack tip.

Another modification of the Griffith-Irwin theory when applied to a ductile material was proposed by Williams (ref. 3). In this ductile-fracture hypothesis, Williams suggests that the exact amount of plastic energy dissipated in the plastically yielded region must be accounted for in computing the critical fracturing force. The shape and volume as well as the stress and plastic strain distribution in the yielded region at the crack tip must then be known a priori in order to apply Williams' hypothesis to ductile materials.

As a somewhat different fracture criterion, McClintock postulates that fracture occurs in a ductile material when a critical strain is reached in a critical volume of the yielded region (ref. 4). The plastically yielded region has also been observed to control the crack-extension rate under fatigue loading, and based on these observations Valluri has proposed a theory on cumulative damage (ref. 5). On the other hand, Liu proposed a theory on the crack-extension rate in fatigue based on the hysteresis energy absorbed in the yielded region (ref. 6).

For each case described above, the shape, stresses, and the total strains in the plastically yielded region at the crack tip must be known before further analytical deductions can be made. Thus, there exists a dire need for detailed information on the states of stresses and strains in these elastic-plastic regions.

Two numerical analyses were conducted on a thin cracked strip under uniaxial tension (refs. 7 and 8), where Mises-Hencky's yield criterion and flow rule due to Prandtl and Reuss were used. The nonlinear elastic-plastic field equations were replaced by the associated finite-difference equations and relaxation techniques were used to solve these equations numerically* in the first paper. In either case, the effects of finite geometries on the crack and the strip width were considered and yield regions were assumed to be relatively large with respect to these geometries. Physically, the results thus obtained corresponded to the elastic-plastic states in the plate composed of an extremely ductile material. It should be noted that Jacobs had solved a similar problem under the condition of plane strain by the finite difference and relaxation method (ref. 10).

Among the other elastic-plastic problems related to cracked structural components, the solution by Hult which deals with a crack in a twisted bar composed of a non-strain hardening material should be noted (ref. 11). Recently, Rice completed a similar analysis in a strain hardening material (ref. 12). Also Koskinen analyzed a grooved bar subjected to longitudinal shear (ref. 13).

In view of the lack of available elastic-plastic solutions for problems involving cracks in thin plates of infinite extent and subjected to tension as well as other modes of loading, namely, in-plane shear in this case, a research program was initiated to obtain elastic-plastic solutions for various cracked structural elements. This report deals with the initial phase of this research

---

* The basic procedure for such numerical analysis was developed by Allen and Southwell (ref. 9).

program which was supported by NASA Grant NsG 532. Two problems were analyzed and the states of stresses in the vicinity of a crack tip were determined for the following loading conditions.

1. A thin infinite plate subjected to uniform tension and composed of elastic, perfectly plastic material.
2. A thin infinite plate subjected to uniform in-plane shear loading and composed of elastic, perfectly plastic material.

SYMBOLS

a	Half crack length of a straight crack
c	yield function
E	modulus of elasticity
G	shear modulus
$2k$	yield stress in tension
K	stress intensity factor
n	integer
r	radial distance from the crack tip
x,y	rectangular coordinates
δ	incremental quantity
ε	strain
θ	angular coordinate
$\Theta =$	$\sigma_{xx} + \sigma_{yy}$
ν	Poisson's ratio
σ	stress or applied uniform tension stress when used without subscripts
τ	applied uniform in-plane shear stress
$\Phi =$	$\sigma_{yy} - \sigma_{xx}$
$\psi =$	$-2\sigma_{xy}$
χ	Airy's stress function
ω	strain function
λ	plastic modulus, a positive constant
∇^2	harmonic operator $\frac{\partial^2}{\partial x^2} + \frac{\partial^2}{\partial y^2}$
∇^4	biharmonic operator $\frac{\partial^4}{\partial x^4} + 2\frac{\partial^4}{\partial x^2 \partial y^2} + \frac{\partial^4}{\partial y^4}$

Superscript

e	elastic component
p	plastic component
t	total quantity

Subscripts

I	uniform tension case
II	uniform in-plane shear case
i	i-th increment
x,y,z	refer to x, y, z coordinates
$\sim$	normalized pseudo stress intensity factor
-	normalized quantity. For the case of uniform tension, all quantities are divided by $\sigma\sqrt{a/2}$. For the case of uniform in-plane shear, all quantities are divided by $\tau\sqrt{2a}$.

DERIVATION OF BASIC EQUATIONS

Introduction

It is assumed that the elastic-plastic boundary of the yield region in the vicinity of the crack tip, although changing in size, will remain relatively the same in shape during successive increase in load. This postulate is based on the assumption that the half crack length, a, is large with respect to the largest radial distance r from the crack tip considered in this analysis, or $a \gg r$. Thus, the problems such as those considered in references 7 and 8 where subsequent growth in the yield zones is influenced by the effects of finite geometries, are excluded.

By determining the shape of the elastic-plastic boundary and the associated state of stresses, the stress distributions at each subsequent increment of increasing load can be determined provided a scaling law is established to relate the size of the elastic-plastic boundary with the applied load.

This basic elastic-plastic state was established by finding a statically admissible stress distribution of the elastic-plastic field in the vicinity of the crack tip. An Airy's stress function, χ, which satisfies the stress equation of compatibility in the elastic region and the Mises-Hencky yield criterion in the plastic region was determined by the method of finite difference combined together with an iterative procedure developed in this program. Some details of this procedure are described in the following sections.

Knowing the elastic-plastic boundary for a given load and with the assumption that the elastic-plastic boundary remains the same in shape but grows in size with increasing applied load as shown in figure 1, it is then possible to determine the numerical value of Airy's stress function at each generic point in the elastic-plastic region with increasing load. Using the flow rule in plasticity, it is also possible to determine the strain distribution in the elastic-plastic region by linear superposition of incremental strain components corresponding to the incremental increase in load.

Statically Admissible Stress Field

When the state of stresses in a plane problem is represented by Airy's stress function $\chi(x,y)$, then in the absence of a body force the stress compatibility equation in the elastic region is satisfied when

$$\nabla^4\chi = 0 \text{ where } \nabla^4 = \frac{\partial^4}{\partial x^4} + 2\frac{\partial^4}{\partial x^2\partial y^2} + \frac{\partial^4}{\partial y^4} \tag{1}$$

and the stresses are represented by

$$\sigma_{xx} = \chi_{,yy}$$

$$\sigma_{yy} = \chi_{,xx} \tag{2}$$

$$\sigma_{xy} = -\chi_{,xy}$$

In the plastically yielded region, the Mises-Hencky yield criterion for an elastic perfectly plastic material in plane stress is

$$\theta^2 + 3(\Phi^2 + \psi^2) = c^2 \tag{3}$$

where $\theta = \sigma_{xx} + \sigma_{yy}$

$\Phi = \sigma_{yy} - \sigma_{xx}$

$\psi = -2\sigma_{xy}$

and $c = 4k$ where $2k$ is the yield stress in uniaxial tension. Using equations (1) and (3), it is then possible to obtain an elastic-plastic solution of a plane stress problem which is statically admissible but in general will not be kinematically admissible. The possibility of the statically admissible solution being also kinematically admissible is governed to a certain extent by appropriate choice of elastic-plastic boundary for a given applied load as well as the method of superimposing successive incremental changes of strains.

In applying the method of finite-difference to determine numerically the stress function, $\chi(x,y)$, a rectangular region in the vicinity of the crack tip was divided into a grid array with equal spacing, h, as shown in figure 2. Using the nodal locations shown in figure 3, equations (2) and (3) are represented in terms of finite difference equations as follows:

In the elastic region, the stress equation of compatibility becomes

$$20\chi_0 - 8(\chi_1 + \chi_2 + \chi_3 + \chi_4) + 2(\chi_5 + \chi_6 + \chi_7 + \chi_8) + \chi_9 + \chi_{10} + \chi_{11} + \chi_{12} = 0 \tag{4}$$

In the plastic region, the Mises-Hencky yield criterion is

$$\theta_0^2 + 3(\phi_0^2 + \psi_0^2) = c^2 \tag{5}$$

where $\theta_0 = \dfrac{\chi_1 + \chi_2 + \chi_3 + \chi_4 - 4\chi_0}{h^2}$

$$\phi_0 = \frac{\chi_1 + \chi_3 - \chi_2 - \chi_4}{h^2}$$

$$\psi_0 = \frac{\chi_5 + \chi_7 - \chi_8 - \chi_6}{2h^2}$$

It is then assumed that the nodes which belong to the yielded region in figure 1 are known a priori. Combining the appropriate boundary conditions such as the applied surface tractions, together with the field equations composed of equation (4) or (5), the unknown stress function, $\chi(x,y)$, at each node can be determined by the array of equations (4) and (5) which will constitute a set of n equations corresponding to a set of n nodes with n unknown χ's. It should be noted that a numerical solution to this set of n algebraic equations is complicated by the nonlinearity of equation (5).

In order to apply linear analysis with a digital computer, the nonlinear equation (5) was modified as follows. For a node in a plastically yielded region, χ is considered to be composed of two parts, namely

$$\chi = \chi^e + \delta\chi \tag{6}$$

where χ^e is the value of the stress function at the particular node for an infinitely elastic material and $\delta\chi$ is the incremental change in the value of the stress function due to plastic yielding. Equation (5) with equation (6) can then be rewritten as

$$\theta_0^{e}\,\delta\theta_0 + 3(\Phi_0^{e}\delta\Phi_0 + \psi_0^{e}\delta\psi_0) = 1/2\,\{c^2 - (\theta_0^{e})^2 - 3[(\Phi_0^{e})^2 + (\psi_0^{e})^2] - (\delta\theta_0)^2 - 3[(\delta\Phi_0)^2 + (\delta\psi_0)^2]\} \tag{7}$$

If $\delta\theta_0$, $\delta\Phi_0$ and $\delta\psi_0$ are relatively small quantities, then as a first approximation the square of these terms can be ignored and equation (7) becomes a linear equation in terms of unknown quantities of $\delta\chi$ due to plastic yielding at the crack tip (ref. 7). Returning to the elastic region, the new value of the stress function at these nodes can also be represented by equation (6) which upon substituting into equation (1) yields

$$\nabla^4\,(\delta\chi) = 0 \tag{8}$$

The approximate form of equation (7) together with equation (8) will yield a set of n linear algebraic equations which can be solved for n unknown quantities of $\delta\chi$ provided χ for the infinitely elastic solid is known.

In order to improve the numerical accuracy of $\delta\chi$, an iteration process was used. The process consisted of computing $\delta\chi$ repeatedly after previous values of $\delta\chi$ were backsubstituted into the righthand side of equation (7). (See Appendix A.) This iteration process converged in general when the estimated yield region was close to what could be expected and when the backsubstituted $\delta\chi$ values were close to the final values of $\delta\chi$. From practical considerations, the number of nonlinear nodes which could be handled satisfactorily by this procedure was approximately four.

Having established the four yield nodes in the rectangular field, a central portion of this field was cut out and the grid distances were halved, as shown in figure 2. The boundary conditions prescribed in this finer meshed grid network were the numerical values established by the coarser grid which accounted for the elastic-plastic state involving four yield nodes. With the fine grid network, the number of yield nodes approximately tripled to twelve nodes. The state of stresses determined by the finite difference method of this mesh side was considered sufficiently accurate since the stress distribution by nature would not change appreciably in the plastic yielded zone.

The iteration process used in the coarse grid analysis described previously would not converge when applied to the fine grid analysis despite the many fruitless efforts involved in conditioning the nonlinear equations.* For small incremental changes in $\delta\chi$, however, the nonlinear terms, $(\delta\theta_0)^2$ etc., could be considered second order quantities. Thus these nonlinear terms in equation (7) were discarded and a different iteration technique was performed by using the following equation:

---

* Numerical difficulties encountered are discussed in reference 15.

$$\theta_0\,\delta\theta_0 + 3(\Phi_0\,\delta\Phi_0 + \psi_0\,\delta\psi_0) = 1/2\,\{c^2 - (\theta_0)^2 - 3[(\Phi_0)^2 + (\psi_0)^2]\} \qquad (9)$$

Note that the superscript of "e" in equation (7) is missing in equation (9) since θ_0, Φ_0, and ψ_0 now correspond to the plastically yielded state determined by the coarse grid analysis. This procedure after considerable manipulation converged to somewhat satisfactory values.

Another procedure attempted was to shift the grid network but maintain the mesh size at h = 1 and to cover the plastic yield region with more nodes. The motivation for this shifted grid procedure was to continue the successful iteration procedure involving four yielded nodes on the assumption that the stress distribution did not change appreciably in the yield zone. This shifted grid procedure which is reported in Appendix B did not yield satisfactory results for this problem.

Having established the necessary field equations suitable for computer analysis, the first step in the numerical analysis was to compute the elastic and initial value of χ^e for each problem. χ^e for the two problems reported here are determined by the use of Westergard's stress functions for a cracked plate subjected to uniform tension and uniform in-plane shear at infinity.

Assuming that the half crack length a is sufficiently large with respect to the elastic-plastic region at the crack tip in figure 2, the stress function χ for a cracked plate subjected to uniform tension, σ, is represented as (ref. 1)

$$\frac{\chi_I^e}{\sigma\sqrt{a/2}} = X_I^e = r^{3/2}\left[\frac{1}{3}\cos\frac{3\theta}{2} + \cos\frac{\theta}{2}\right] \qquad (10)$$

where r and θ are local polar coordinates with origin at the crack tip as shown in figure 4. X^e is a normalized stress function independent of the half crack length. For a plate loaded with uniform in-plane shear, τ, the normalized stress function, can be represented as

$$\frac{\chi_{II}^e}{\tau\sqrt{2a}} = X_{II}^e = -r^{3/2}\left(\sin\theta\cos\frac{\theta}{2}\right) . \qquad (11)$$

If it can be further assumed that the plastic region is sufficiently small with respect to the elastic-plastic region, then the small plastic region in the center of the rectangular region will not affect values of X^e on the exterior boundaries of the region. The first step in the numerical procedure then is to compute X^e by equation (10) or (11) and then prescribe these X^e along the nodes on the exterior boundaries. X^e values at location one grid distance outside of the exterior boundary are also needed for finite difference analysis of a biharmonic equation.

Incremental Growth of Elastic-Plastic Boundary

Having established the statically admissible stress field for one particular load, the stress function for each increment of increasing load can be easily obtained by observation of equations (10) and (11). Since the prescribed χ^e on the rectangular boundary is inversely proportional to the applied load σ or τ, the effect of an increase in σ or τ can be accounted for by an appropriate increase in the size of the rectangular boundaries as shown in figure 1. $\delta\chi$ or $\chi = \chi^e + \delta\chi$ as well as the elastic-plastic boundary will remain the same for a point in the same position relative to the enlarged rectangular region. For a stationary generic point in the elastic-plastic region, the stress function and the state of stress can then be determined as a function of increasing load.

At a generic point in the elastic-plastic region, the change in the stress function per incremental loading of the nth step can be represented as

$$\chi = \chi^e + \delta\chi^{(1)} + \delta\chi^{(2)} + \ldots + \delta\chi^{(n)} \tag{12}$$

Postulating a flow rule for the stress-strain relation in the plastically yielded region, the nth incremental change in the strains can be represented as

$$\begin{aligned}
\delta\varepsilon_{xx}^{(n)} &= \frac{1}{E}\left[\delta\sigma_{xx}^{(n)} - \nu\delta\sigma_{yy}^{(n)}\right] + \delta\lambda^{(n)}\left[2\sigma_{xx}^{(n)} - \sigma_{yy}^{(n)}\right] \\
\delta\varepsilon_{yy}^{(n)} &= \frac{1}{E}\left[\delta\sigma_{yy}^{(n)} - \nu\delta\sigma_{xx}^{(n)}\right] + \delta\lambda^{(n)}\left[2\sigma_{yy}^{(n)} - \sigma_{xx}^{(n)}\right] \\
\delta\varepsilon_{zz}^{(n)} &= -\frac{\nu}{E}\left[\delta\sigma_{xx}^{(n)} + \delta\sigma_{yy}^{(n)}\right] - \delta\lambda^{(n)}\left[\sigma_{xx}^{(n)} + \sigma_{yy}^{(n)}\right] \\
\delta\varepsilon_{xy}^{(n)} &= \frac{1+\nu}{E}\,\delta\sigma_{xy}^{(n)} + 3\,\delta\lambda^{(n)}\,\sigma_{xy}^{(n)}
\end{aligned} \tag{13}$$

where E and ν are elastic modulus of elasticity and the Poisson's ratio respectively and $\delta\lambda^{(n)}$ is an undetermined constant of flow.

$\delta\sigma^{(n)}$, ..., and $\sigma^{(n)}$, ... are known from our previous analysis. Also, from the strain compatibility relation, $\delta\lambda^{(n)}$ can be determined as

$$\delta\lambda^{(n)} = -\frac{\nabla^4\,\delta\chi^{(n)}}{2E\nabla^4\left(\chi^e + \delta\chi^{(1)} + \delta\chi^{(2)} + \ldots + \delta\chi^{(n)}\right)} \tag{14}$$

Knowing $\delta\lambda^{(n)}$ then, it is possible to compute the four incremental strain components by equation (13). This portion of the computation was not performed since $\delta\lambda$ could not be determined with sufficient accuracy to carry out this computation.

Numerical Procedure and Results

The first step in the elastic-plastic analysis is to yield the most obvious point, namely the node at the crack tip by estimating a value of $\underline{c}^2$(normalized function of yield stress) in equation (7) for this node. The remaining nodes are assumed elastic and therefore equation (8) is assigned to these nodes and $\delta\underline{\chi}$ is determined by linear analysis combined with the iteration procedure described previously.

If the material is weakened, the strain energy stored in the vicinity of the crack tip is distributed to adjacent areas; hence, more nodes undergo yielding and the plastic enclave is enlarged. With the value of $\underline{c}^2$ for one-node plastic enclave, plastic enclave which includes four yielded nodes was established and a new $\underline{c}^2$ was estimated. The numerical method described previously was carried out again with the exception that four nonlinear equations were used in the iteration. The results of the stress functions, stresses, and $\underline{c}^2$ computed are shown in figures 5 to 10.

As mentioned previously the plastic enclave could not be enlarged further to take in more yielded nodes, since the iteration procedure diverged numerically for more than four yielded nodes. Therefore, the original grid (h = 1) was halved into a finer mesh (h = 1/2). In order to keep the size of the computer program within its storage capacity and to allow interchangeability in computer program of one grid mesh to the other, only one quarter of the original region was considered in the fine grid analysis. Complete linear analysis plus successive matrix inversion technique in place of iteration procedure was employed in the fine grid analysis. Details of this procedure are found in reference 15.

The numerical values of stress function thus obtained together with the stresses and $\underline{c}^2$ which were calculated by finite difference are shown in figures 11 to 16. Although the assigned maximum value of $\underline{c}^2$ for this calculation was 4.17, higher values of $\underline{c}^2$ were obtained in the plastically yielded region in figure 16. This discrepancy somewhat indicates the inadequacy of the numerical procedure employed here. Despite this discrepancy, the sufficiently continuous values of the stresses and the stress function leads one to believe that these values are substantially correct within the first two significant figures.

Cracked Plate Subjected to Uniform In-Plane Shearing

Except for equation (11), similar numerical procedures as described above were used to determine the stress function, stresses, and $\underline{c}^2$ distribution in the coarse and fine grid analyses. Figures 17 through 22 and figures 23 through 28 show these distributions for regions with grid spacing of h = 1 and a subregion with a grid spacing of h = 1/2. Again, the discrepancy between the calculated $\underline{c}^2$ and the assigned maximum value of $\underline{c}^2$ = 2.87 is to be noted in figure 28.

DISCUSSION

As noted in the first section, the intention of this investigation was to establish a ductile fracture criterion. With the intention of extending the Griffith-Irwin theory of fracture into ductile fracture following Irwin's yield correction factor, the numerical results were compared with equivalent elastic results.

Figures 29 through 32 show the stress function versus radial distances from the crack tip for the two problems. These figures show that on a log-log plot, the stress function remains essentially a straight line with a slope of close to m = 1.5. The values of m - 2 represent the negative power of r or the order in which the stresses increase as they approach the crack tip. Tables I and II show the slopes of these lines fitted through points in figures 29 through 32 by the method of least square. Normalized pseudo stress intensity factors were then determined from these fitted lines as

$$\underset{\sim}{K}_I = \frac{r^{-m}\, \underset{\sim}{X}_I}{\frac{1}{3}\cos\frac{3\theta}{2} + \cos\frac{\theta}{2}} \qquad \text{for uniform tension} \qquad (15)$$

$$\underset{\sim}{K}_{II} = -\frac{r^{-m}\, \underset{\sim}{X}_{II}}{\sin\theta \cdot \cos\frac{\theta}{2}} \qquad \text{for uniform in-plane shear} \qquad (16)$$

These values are also tabulated in Tables I and II.

From the above results it can be seen that the stress singularity of $r^{-1/2}$ is essentially maintained at a small distance away from the crack tip and thereafter. Thus, the states of stresses in these two problems can be represented in the form of equation (10) or (11) with a magnification factor of 1.05 to 1.10 for regions ahead of the crack tips. Details of the latter values are shown in figures 33 and 34.

Irwin proposed that the plasticity effect can be handled by increasing the effective crack length for the state of plane stress from a to $a\left(1 + \frac{\sigma^2}{4\sqrt{2}\, 4k^2}\right)$ (ref. 2). The stress intensity factor determined by Irwin's correction for the tension problem will be

$$K = \sqrt{\pi}\,\sigma\,\sqrt{a}\,\sqrt{1 + \frac{\sigma^2}{4\sqrt{2}\,\sigma_o^2}} \doteq \sqrt{\pi}\,\sigma\,\sqrt{a}\left(1 + 0.088\,\frac{\sigma^2}{4k^2}\right) \qquad (17)$$

For a nominal loading condition of $\frac{\sigma}{2k} = 0.7$, equation (17) yields K = 1.05 which is in the realm of the correction factor obtained by this analysis.

APPENDIX A

A flow chart of the computer program is shown on the next page to help to visualize the iteration procedure described in the main text.

FLOW CHART:

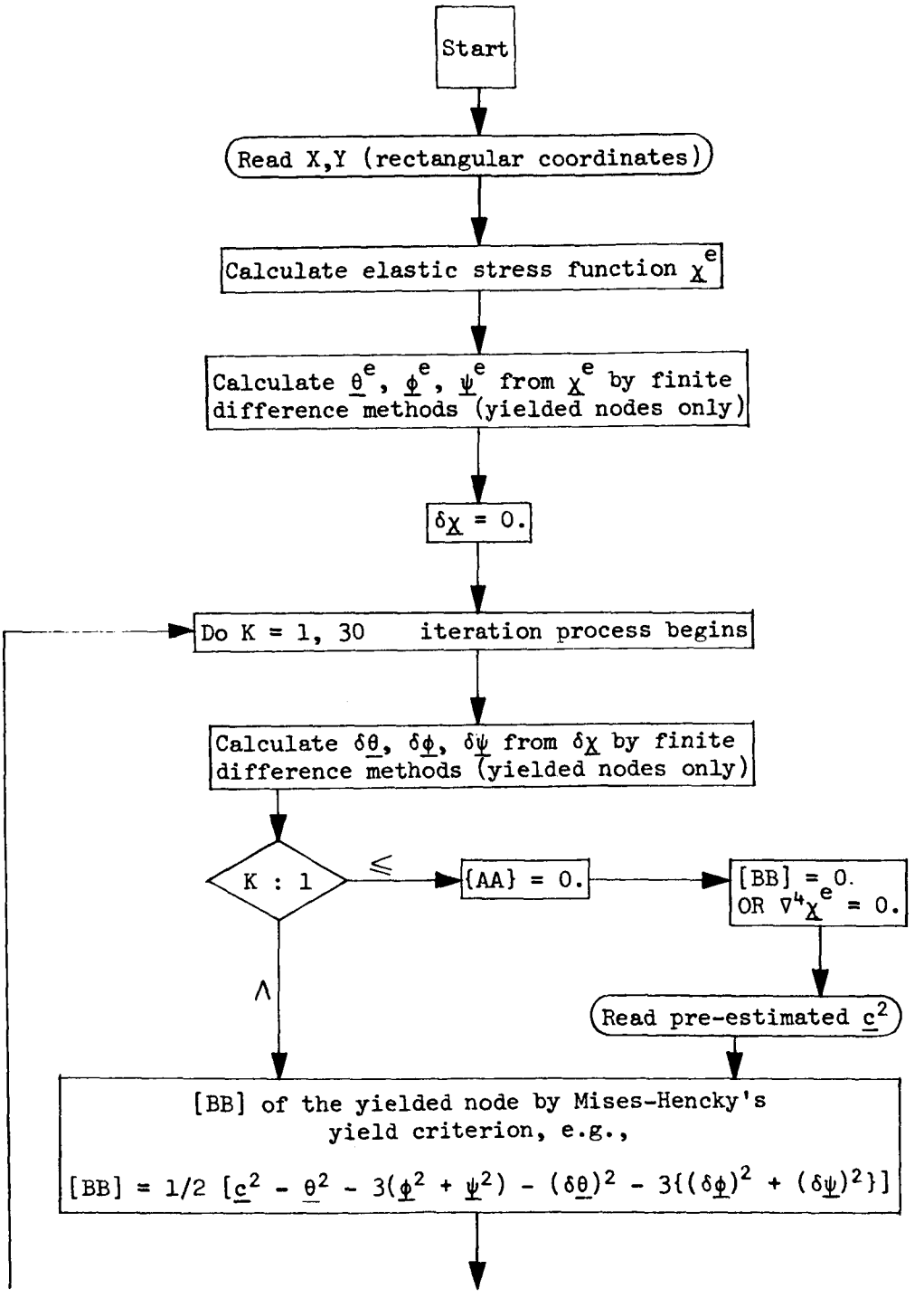
Start
Read X,Y (rectangular coordinates)
Calculate elastic stress function $\underline{\chi}^e$
Calculate $\underline{\theta}^e$, $\underline{\phi}^e$, $\underline{\psi}^e$ from $\underline{\chi}^e$ by finite difference methods (yielded nodes only)
$\delta\underline{\chi} = 0.$
Do K = 1, 30 iteration process begins
Calculate $\delta\underline{\theta}$, $\delta\underline{\phi}$, $\delta\underline{\psi}$ from $\delta\underline{\chi}$ by finite difference methods (yielded nodes only)
K : 1
≤
{AA} = 0.
[BB] = 0.
OR $\nabla^4\underline{\chi}^e = 0.$
Read pre-estimated $\underline{c}^2$
Λ
[BB] of the yielded node by Mises-Hencky's yield criterion, e.g.,
[BB] = 1/2 [$\underline{c}^2 - \underline{\theta}^2 - 3(\underline{\phi}^2 + \underline{\psi}^2) - (\delta\underline{\theta})^2 - 3\{(\delta\underline{\phi})^2 + (\delta\underline{\psi})^2\}$]

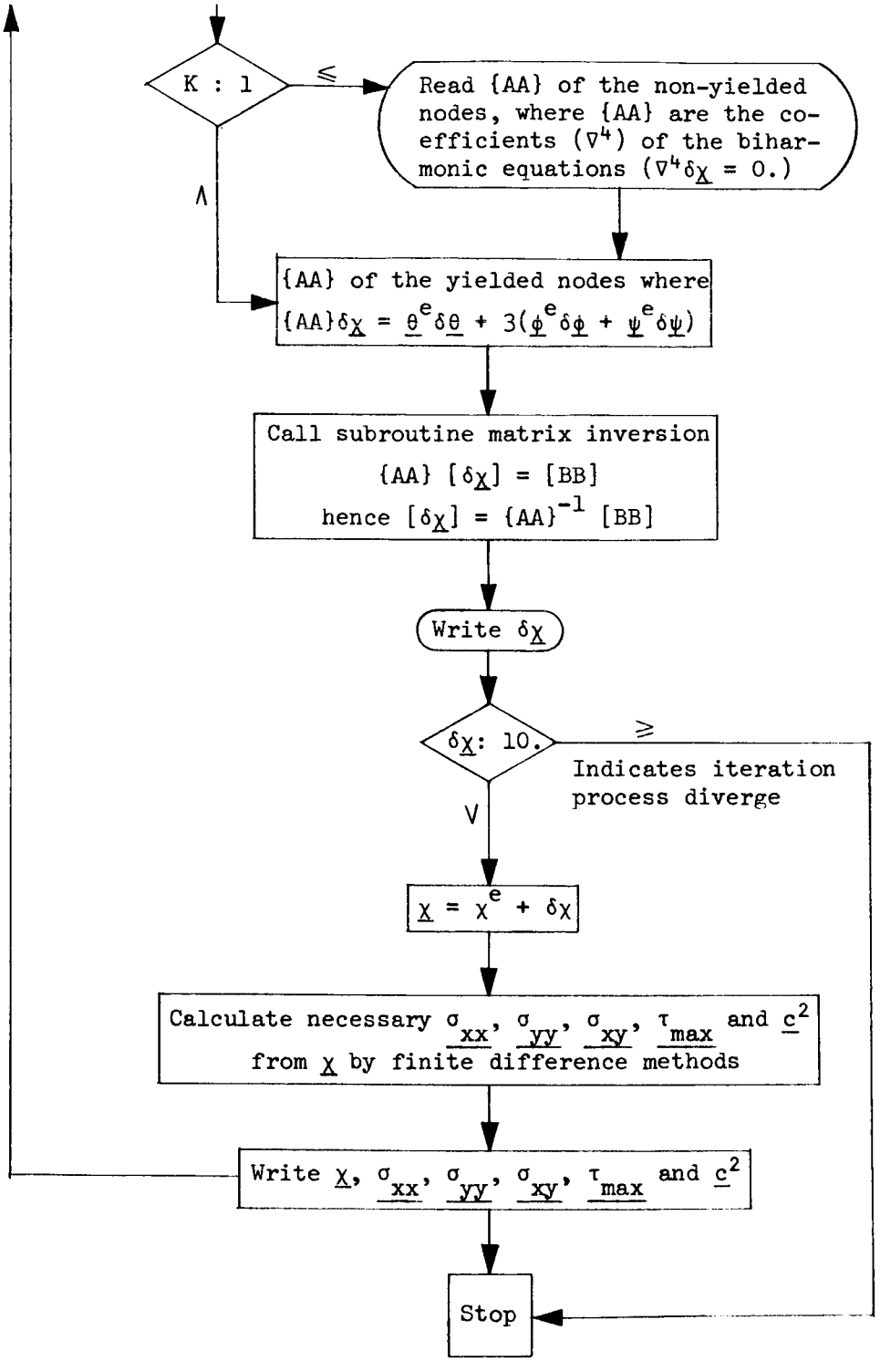
K : 1
≤
Read {AA} of the non-yielded nodes, where {AA} are the coefficients (∇^4) of the biharmonic equations ($\nabla^4 \delta\underline{\chi} = 0.$)
∧
{AA} of the yielded nodes where
$\{AA\}\delta\underline{\chi} = \underline{\theta}^e\delta\underline{\theta} + 3(\underline{\phi}^e\delta\underline{\phi} + \underline{\psi}^e\delta\underline{\psi})$
Call subroutine matrix inversion
$\{AA\}\ [\delta\underline{\chi}] = [BB]$
hence $[\delta\underline{\chi}] = \{AA\}^{-1}\ [BB]$
Write $\delta\underline{\chi}$
$\delta\underline{\chi}$: 10.
≥
Indicates iteration process diverge
∨
$\underline{\chi} = \chi^e + \delta\chi$
Calculate necessary $\sigma_{\underline{xx}}$, $\sigma_{\underline{yy}}$, $\sigma_{\underline{xy}}$, $\tau_{\underline{max}}$ and $\underline{c}^2$ from $\underline{\chi}$ by finite difference methods
Write $\underline{\chi}$, $\sigma_{\underline{xx}}$, $\sigma_{\underline{yy}}$, $\sigma_{\underline{xy}}$, $\tau_{\underline{max}}$ and $\underline{c}^2$
Stop

APPENDIX B

The procedure which appeared moderately successful was the procedure of the shifting of the coarse finite difference grid. By parallel and perpendicular shifting of the coarse grid in the region, it is possible to obtain an estimate of the stress function at any particular point in the region. This procedure has the advantage of assured convergence because the number of plastically yielded nodal points was confined to approximately four or five points. Obviously, the use of such coarse finite difference grid could yield only average values of the state of stresses. Fluctuations of the state of stresses in the plastically yielded region were believed to be sufficiently small such that the results thus obtained could not be in substantial error.

Figures 35 and 36 show stress component $\underline{\sigma}_{yy}$ and $\underline{c}^2$ computed by this procedure. As self evident, the state of stresses determined by this procedure was not sufficiently smooth and continuous to continue with this procedure. It is believed, however, that the shifted grid approach could find application in other elastic-plastic problems with relatively small stress gradients.

APPENDIX C

Another approach was to use stable numerical results obtained by the coarse grid finite difference network for the stress distribution and to develop a curve fitting procedure to the strain function separately. In an elastic-plastic analysis where the stress singularity is removed, it seems reasonable to assume that the state of stresses will not vary rapidly and therefore the state of stresses obtained by a coarse finite difference grid network should be a fair representation of the true state of stresses. The state of stresses would thus be determined by linear interpolation of the results obtained by the coarse grid work.

The strain function, which will represent the total strain at all points, must be biharmonic from the compatibility of the total strains. For an Airy stress function, χ, which is biharmonic and which satisfies the following relation,

$$\sigma_{xx} = \chi_{,yy} \qquad \sigma_{yy} = \chi_{,xx} \qquad \sigma_{xy} = -\chi_{,xy}$$

a similar strain function can be determined as

$$\epsilon_{xx} = \frac{1}{E} [\omega_{,yy} - \nu \cdot \omega_{,xx}]$$

$$\epsilon_{yy} = \frac{1}{E} [\omega_{,xx} - \nu \cdot \omega_{,yy}]$$

$$\epsilon_{xy} = - \frac{1+\nu}{E} \omega_{,xy}$$

In the elastic region, the strain function as defined above will coincide with the stress function or $\chi = \omega$. In the plastically yielded region, however, the two functions will differ.

A plot of stress function obtained from the finite difference analysis with respect to distance, r, from the crack tip, shows that possibly

$$\omega(r,\theta) = \omega_1(\frac{1}{r}) \cdot \omega_1(\theta) + \omega_2 (\frac{1}{\sqrt{r}}) \cdot \omega_2(\theta)$$

in the elastic region. Assuming that the same trend holds true in the plastically yielded region, a strain function which is equal to the stress function in the elastic region could be determined.

The state of strain was determined from this strain function and checks were made if the Prandtl-Reuss flow rule can be satisfied between the states of stresses and strains thus determined. The results turned out to be negative and this approach was also abandoned.

REFERENCES

1. Irwin, G. R.: Fracture. Vol. 6 (Elasticity and Plasticity) Handbuch der Physik, Springer (Berlin), 1958, pp. 551-590.

2. Irwin, G. R.: Fracture Testing of High Strength Sheet Materials. ASTM Bulletin, Jan. 1960, pp. 29-40.

3. Williams, M. L.: Some Observations Regarding the Stress Field Near the Point of a Crack. Proc. of the Crack Propagation Symposium, Cranfield, England, Sept. 1961.

   Also: A Review of Recent Research at GALCIT Concerning Fracture Initiation. Aero. Research Lab. TN, April 1961.

4. McClintock, F. A.: Ductile Fracture Instability in Shear. J. of Appl. Mech., vol. 25, no. 4, Dec. 1958, pp. 582-588.

5. Valluri, S. R.: A Theory of Cumulative Damage in Fatigue. Aero. Research Lab. TN, Jan. 1961.

6. Liu, H. W.: Fatigue Crack Propagation and Applied Stress Range--An Energy Approach, J. of Basic Eng., vol. 85, series D, no. 1, March 1963, pp. 116-122.

7. Stimpson, L. D.; and Eaton, D. M.: The Extent of Elastic-Plastic Yielding at the Crack Point of an Externally Notched Plane Stress Tensile Specimen. Guggenheim Aero. Lab. of Cal. Institute of Tech. Report SM 60-10, June 1960.

8. Swedlow, J. L.; Williams, M. L.; and Yang, W. H.: Elasto-Plastic Stresses and Strains in Cracked Plates. Proc. of Int'l. Conf. on Fracture, Sendai, Japan, Sept. 1965.

9. Allen, D. N. de G.; and Southwell, R. V.: Plastic Straining in Two-Dimensional Stress Systems. Philosoph. Trans. of the Roy. Soc. (London), series A, vol. 242, June 1950, pp. 379-414.

10. Jacobs, J. A.: Relaxation Methods Applied to Problems of Plastic Flow I, Notched Bar under Tension. Philosoph. Mag., vol. 41, 1950, pp. 349-361.

11. Hult, J. A. H.: Fatigue Crack Propagation in Torsion. J. of the Mech. and Physics of Solids, vol. 6, 1957, pp. 47-52.

12. Rice, J. R.: Stresses Due to Sharp Notch in a Work Hardening Elastic-Plastic Material Loaded by Longitudinal Shear, Brown Univ. TR, Dec. 1956.

13. Koskinen, M. F.: Elastic Plastic Deformation of a Single Grooved Flat Plate under Longitudinal Shear. ASME paper no. 62-WA-137, presented at Winter Annual Meeting of ASME, Nov. 25-30, 1965.

14. Roberts, E., Jr.; and Mendelson, A.: Analysis of Plastic Thermal Stresses and Strains in Finite Thin Plate of Strain Hardening Material. NASA TN D-2206, Oct. 1964.

15. Woo, Savio: Elastic Plastic Analysis in the Vicinity of a Crack Tip. Univ. of Washington, MS Thesis, Dec. 1966.

TABLE I-a

UNIFORM TENSION LOADING

COARSE GRID

θ	m	$K_{\sim I}$
0°	1.36	1.19
26.6°	1.45	1.18
45.0°	1.50	1.12
63.4°	1.53	1.03
90.0°	1.58	.965
116.6°	1.74	.744
135.0°	2.19	.281

TABLE I-b

UNIFORM TENSION LOADING

FINE GRID

θ	m	$K_{\sim I}$
0°	1.35	1.08
26.6°	1.40	1.16
45.0°	1.46	1.17
63.4°	1.50	1.06
90.0°	1.59	.969
116.6°	1.75	.794
135.0°	1.93	.562

TABLE II-a

UNIFORM IN-PLANE SHEAR LOADING

COARSE GRID

θ	m	$\underset{\sim}{K}_{II}$
26.6°	1.41	1.14
45°	1.42	1.13
63.4°	1.42	1.11
90°	1.38	1.17
116.6°	1.40	1.15
135°	1.40	1.18
153.4°	1.43	1.14

TABLE II-b

UNIFORM IN-PLANE SHEAR LOADING

FINE GRID

θ	m	$\underset{\sim}{K}_{II}$
26.6°	1.35	1.18
45°	1.44	1.07
63.4°	1.45	1.07
90°	1.40	1.08
116.6°	1.44	1.09
135°	1.42	1.11
153.4°	1.33	1.28

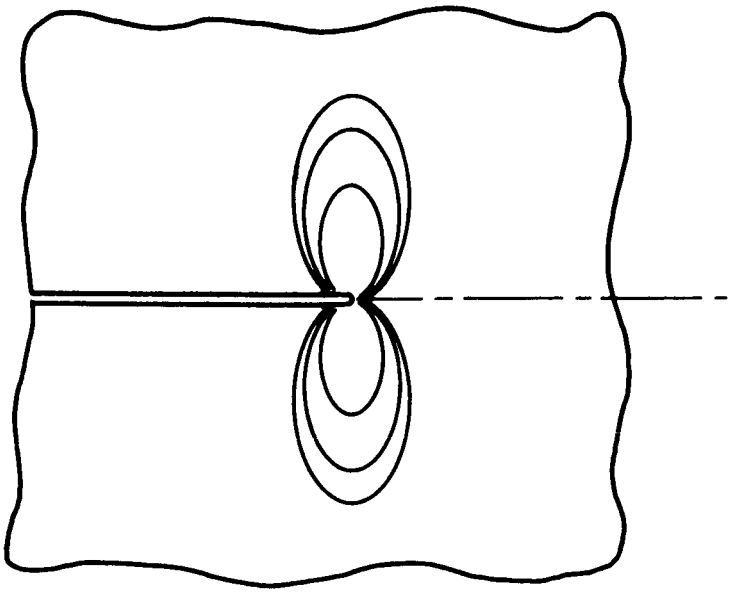

FIGURE 1. GROWTH OF ELASTIC-PLASTIC BOUNDARY WHEN MATERIAL IS WEAKENED WITH CONSTANT APPLIED LOAD

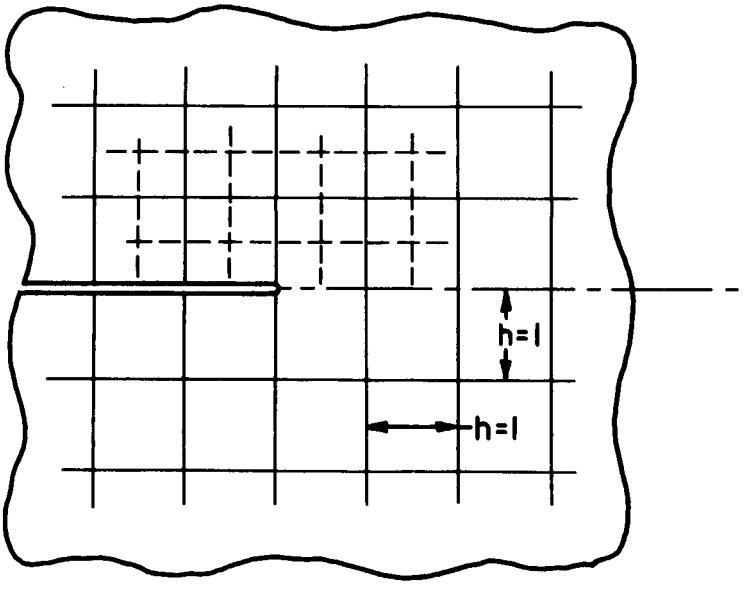

FIGURE 2. FINITE DIFFERENCE GRID IN THE VICINITY OF A CRACK TIP

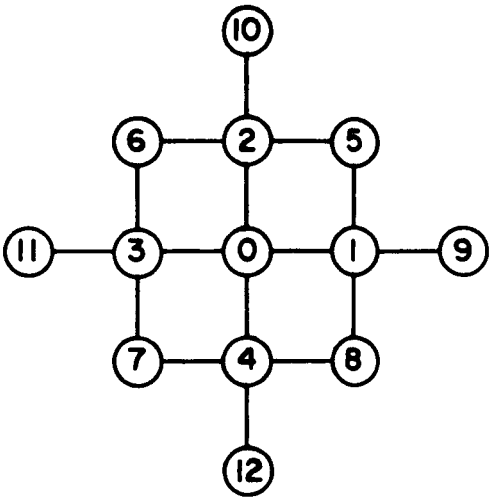

FIGURE 3. NODAL LOCATION FOR BI-HARMONIC FINITE DIFFERENCE OPERATOR

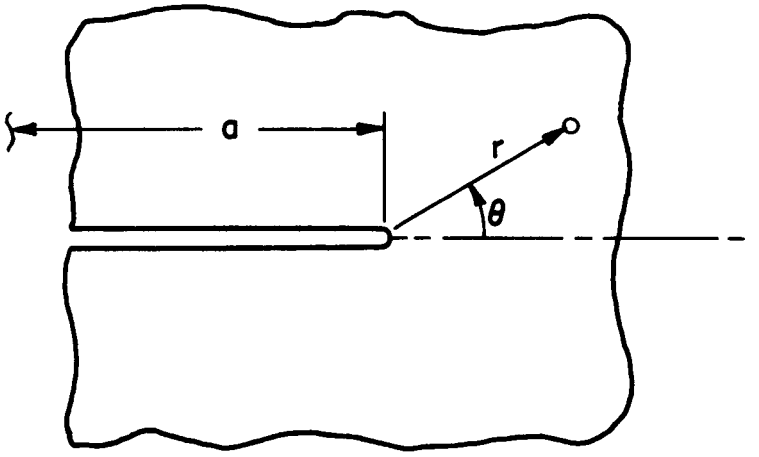

FIGURE 4. LOCAL POLAR COORDINATES IN THE VICINITY OF A CRACK TIP

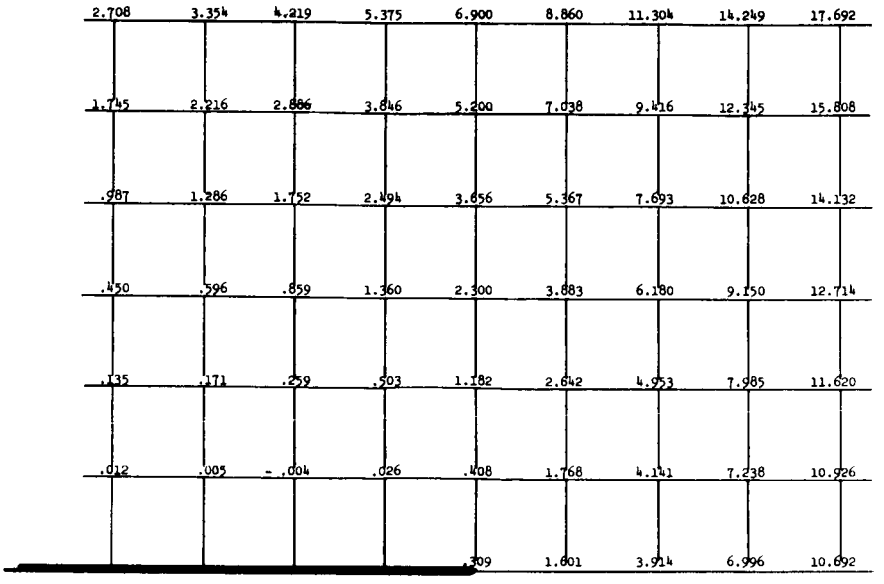

FIGURE 5. X_1 DISTRIBUTION IN CRACKED PLATE SUBJECTED TO UNIFORM TENSION
ELASTIC-PLASTIC BOUNDARY AT $\zeta^2 = 3.25$
COARSE GRID (GRID LENGTH $h = 1$)

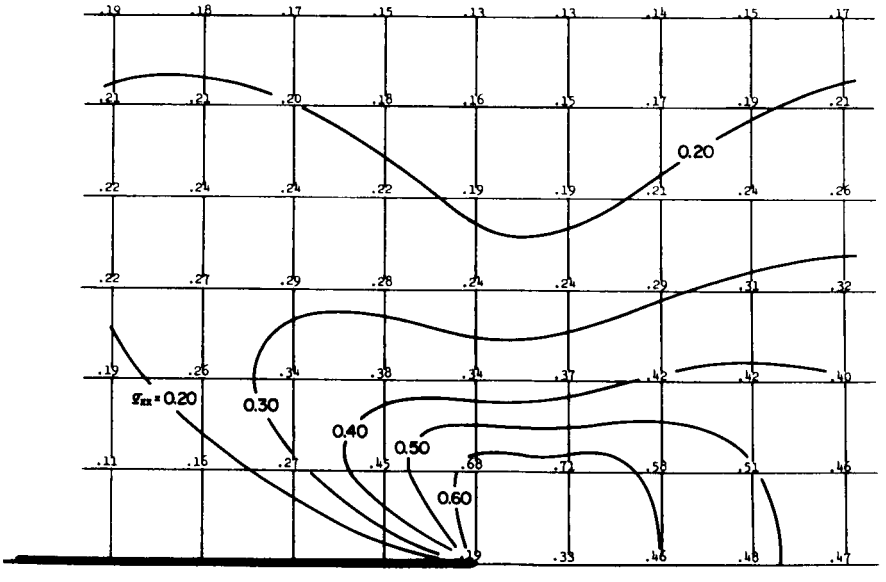

FIGURE 6. σ_{xx} DISTRIBUTION IN CRACKED PLATE SUBJECTED TO UNIFORM TENSION
ELASTIC-PLASTIC BOUNDARY AT $\zeta^2 = 3.25$
COARSE GRID (GRID LENGTH $h = 1$)

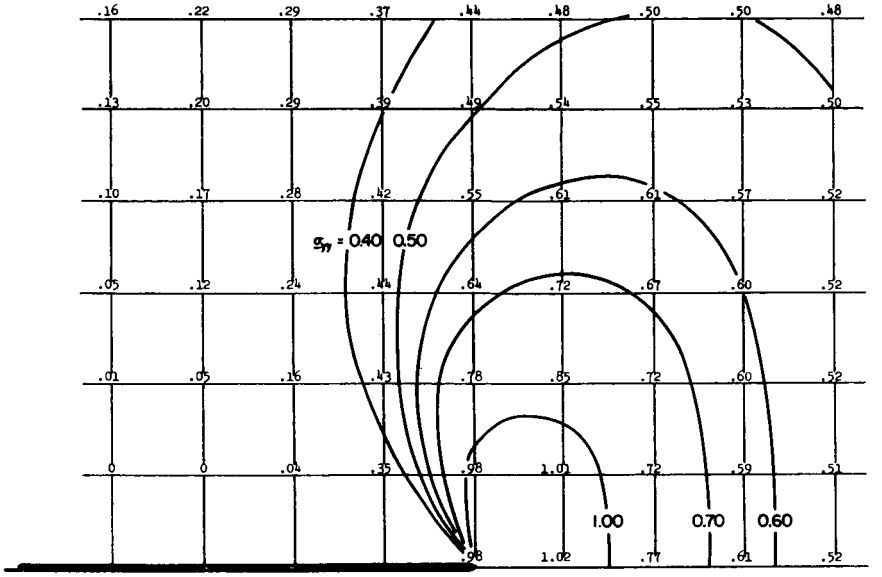

FIGURE 7. σ_{yy} DISTRIBUTION IN CRACKED PLATE SUBJECTED TO UNIFORM TENSION
ELASTIC-PLASTIC BOUNDARY AT $\zeta^2 = 3.25$
COARSE GRID (GRID LENGTH h = 1)

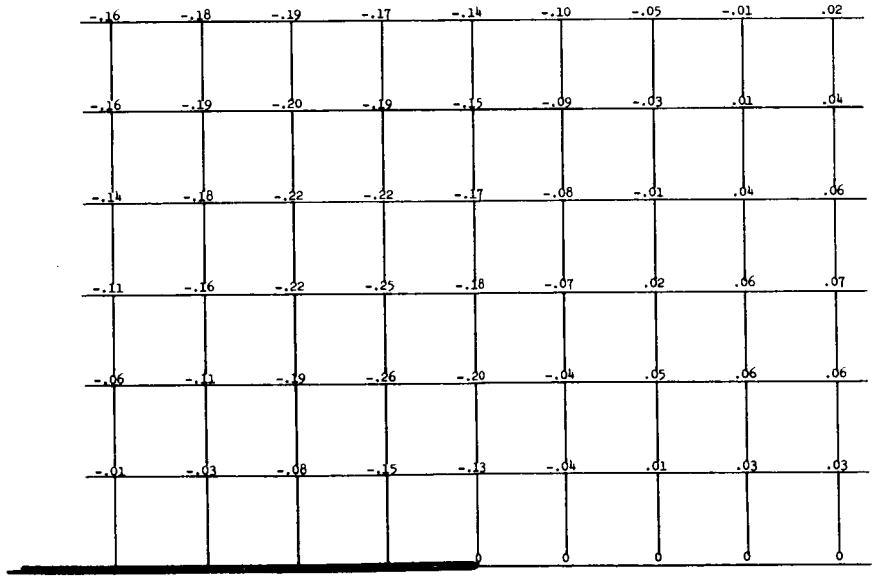

FIGURE 8. σ_{xy} DISTRIBUTION IN CRACKED PLATE SUBJECTED TO UNIFORM TENSION
ELASTIC-PLASTIC BOUNDARY AT $\zeta^2 = 3.25$
COARSE GRID (GRID LENGTH h = 1)

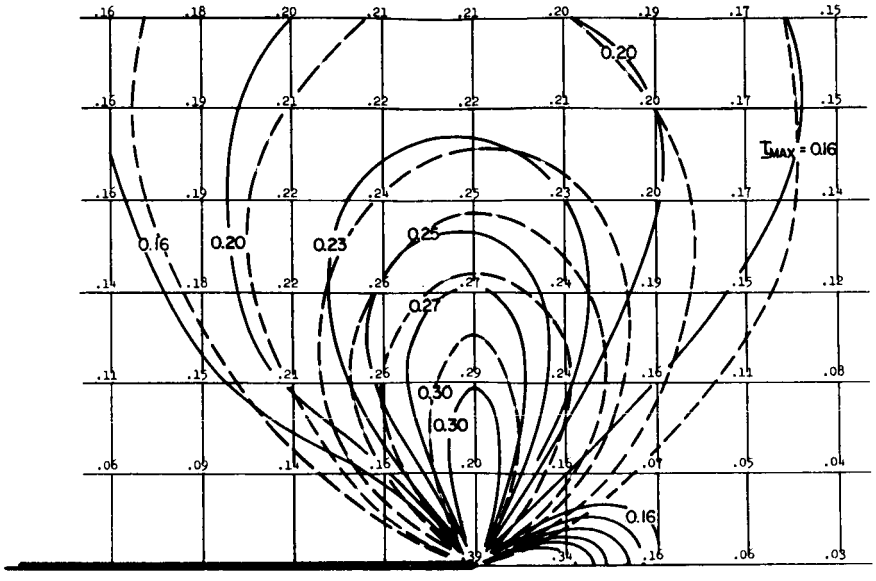

FIGURE 9. τ_{max} DISTRIBUTION IN CRACKED PLATE SUBJECTED TO UNIFORM TENSION
ELASTIC-PLASTIC BOUNDARY AT $\zeta^2 = 3.25$
COARSE GRID (GRID LENGTH h = 1) ; SOLID LINES = ELASTIC-PLASTIC ANALYSIS ; DASHED LINES = ELASTIC ANALYSIS

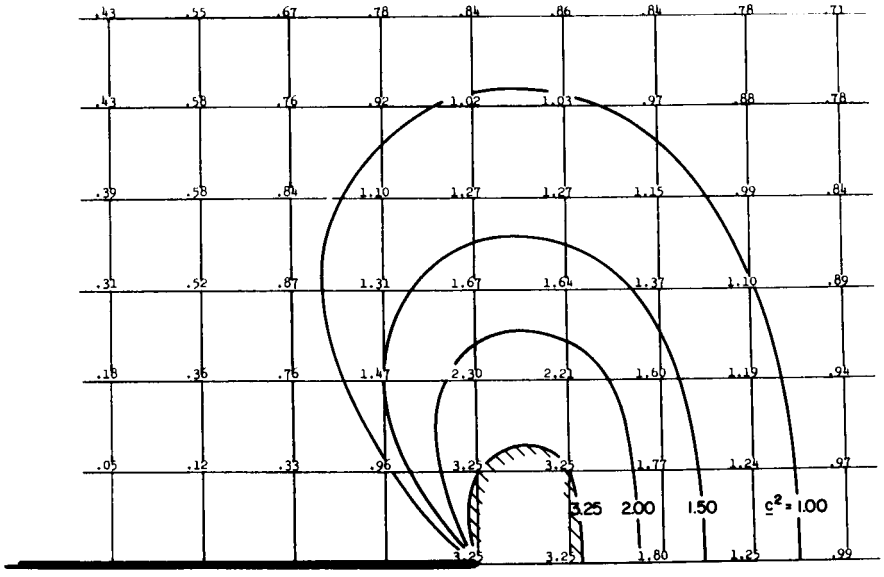

FIGURE 10. ζ^2 DISTRIBUTION IN CRACKED PLATE SUBJECTED TO UNIFORM TENSION
ELASTIC-PLASTIC BOUNDARY AT $\zeta^2 = 3.25$
COARSE GRID (GRID LENGTH h = 1)

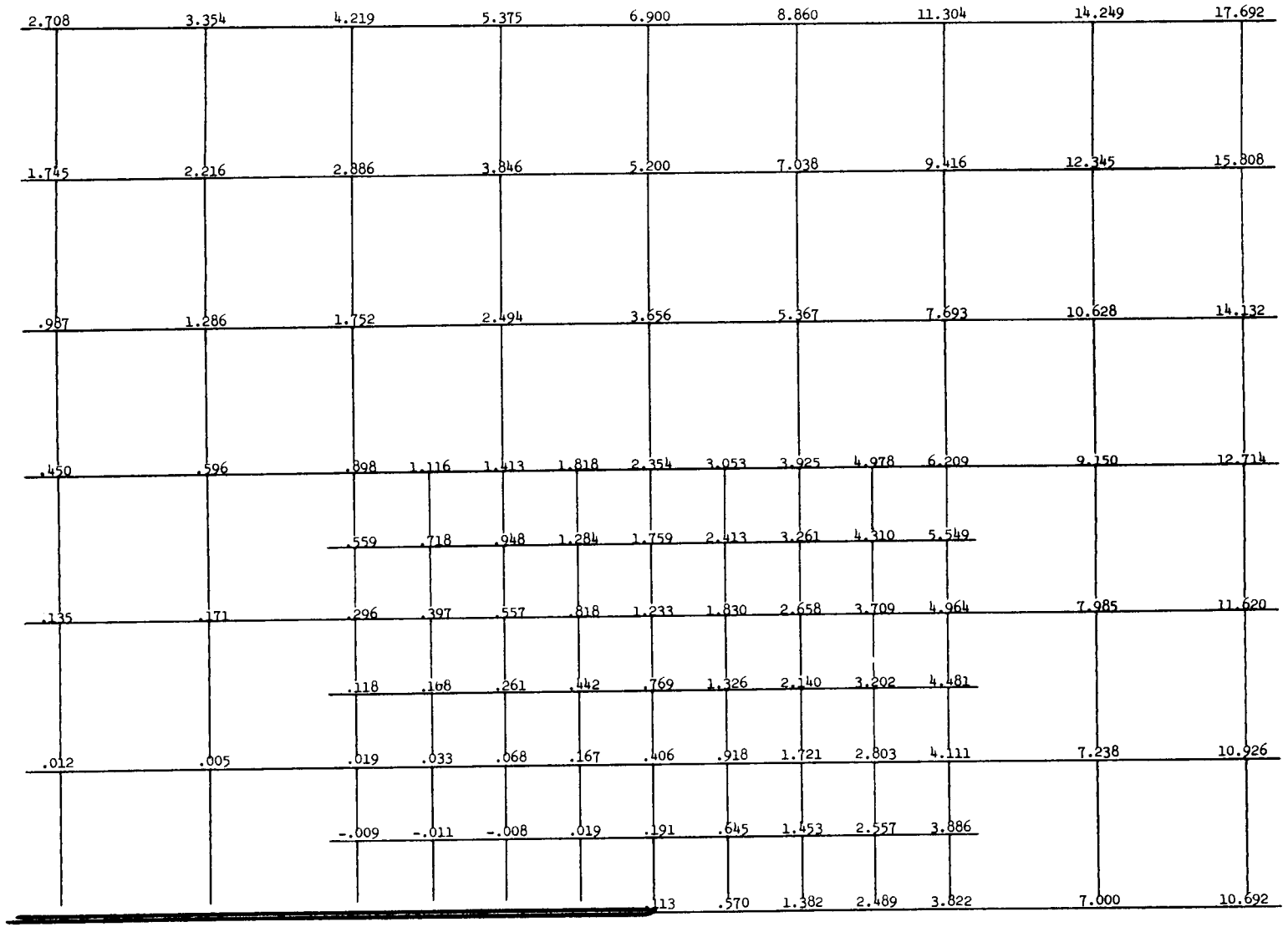

FIGURE 11. $\underline{X}_1$ DISTRIBUTION IN CRACKED PLATE SUBJECTED TO UNIFORM TENSION

ELASTIC-PLASTIC BOUNDARY AT $\varsigma^2 = 4.17$

FINE GRID (GRID LENGTH h = 1/2) ; COARSE GRID (h = 1)

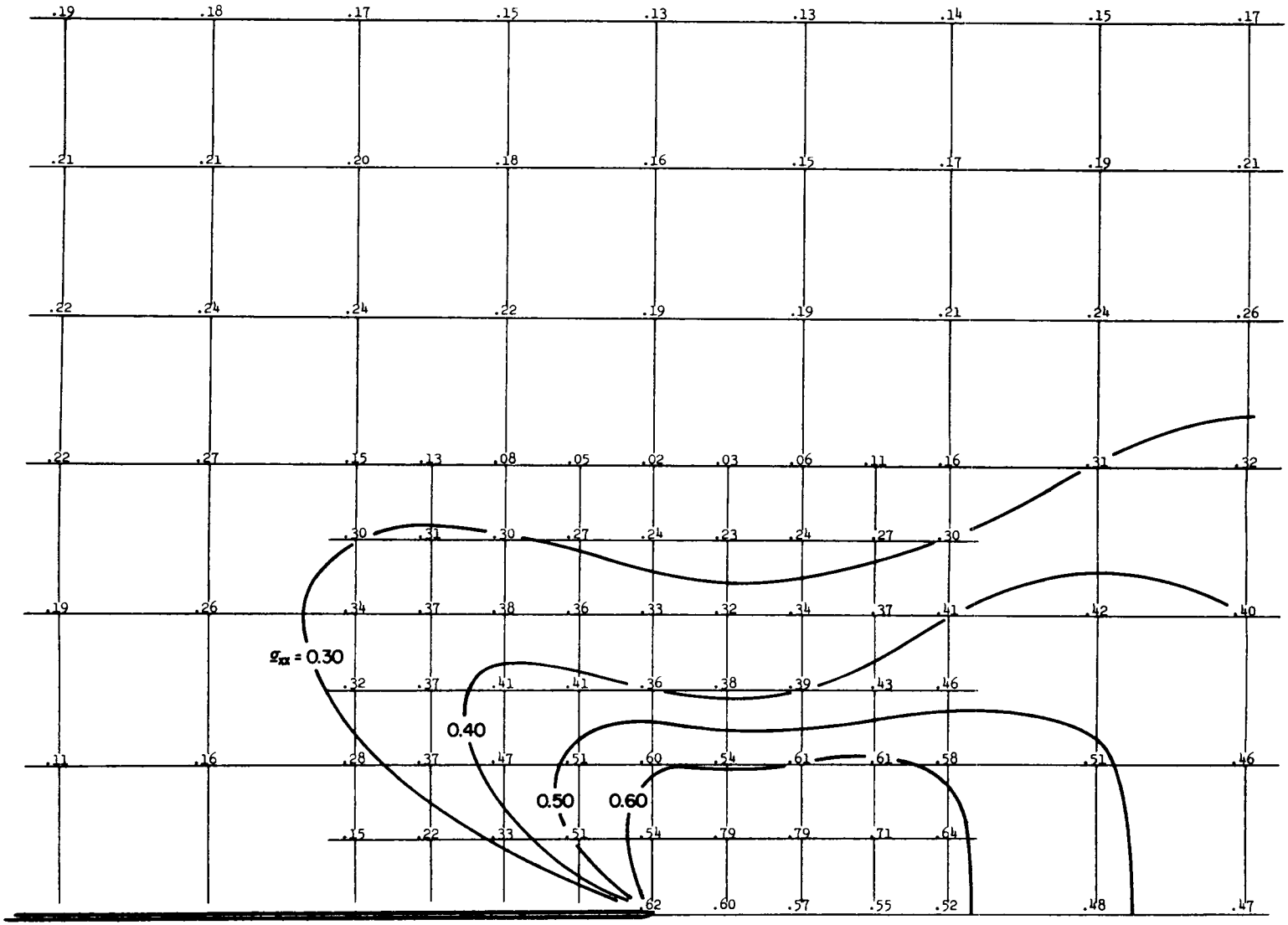

FIGURE 12. σ_{xx} DISTRIBUTION IN CRACKED PLATE SUBJECTED TO UNIFORM TENSION

ELASTIC-PLASTIC BOUNDARY AT $\xi^2 = 4.17$

FINE GRID (GRID LENGTH h = 1/2) ; COARSE GRID (h=1)

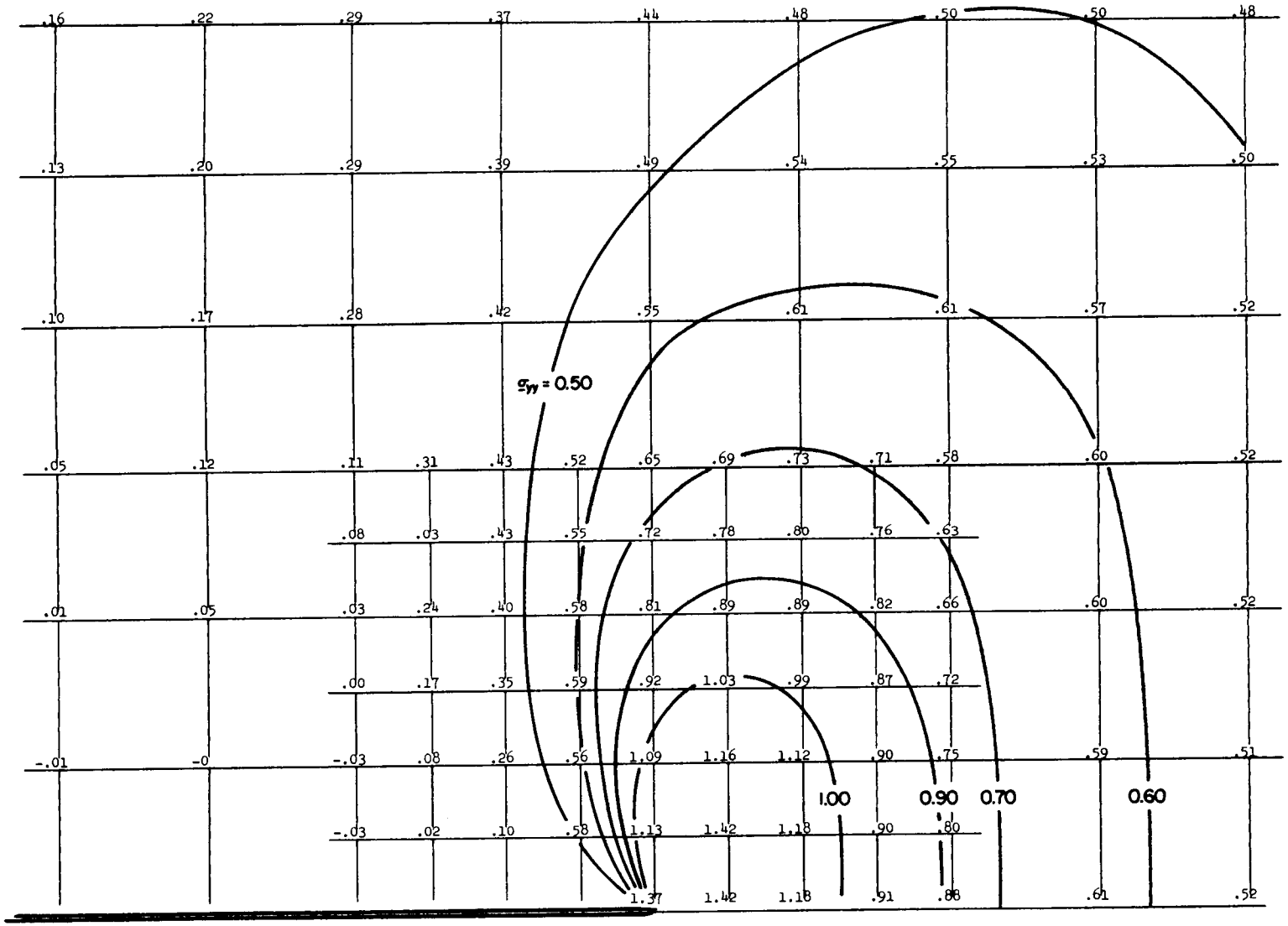

FIGURE 13. σ_{yy} DISTRIBUTION IN CRACKED PLATE SUBJECTED TO UNIFORM TENSION

ELASTIC-PLASTIC BOUNDARY AT $\zeta^2 = 4.17$

FINE GRID (GRID LENGTH h = 1/2) ; COARSE GRID (h = 1)

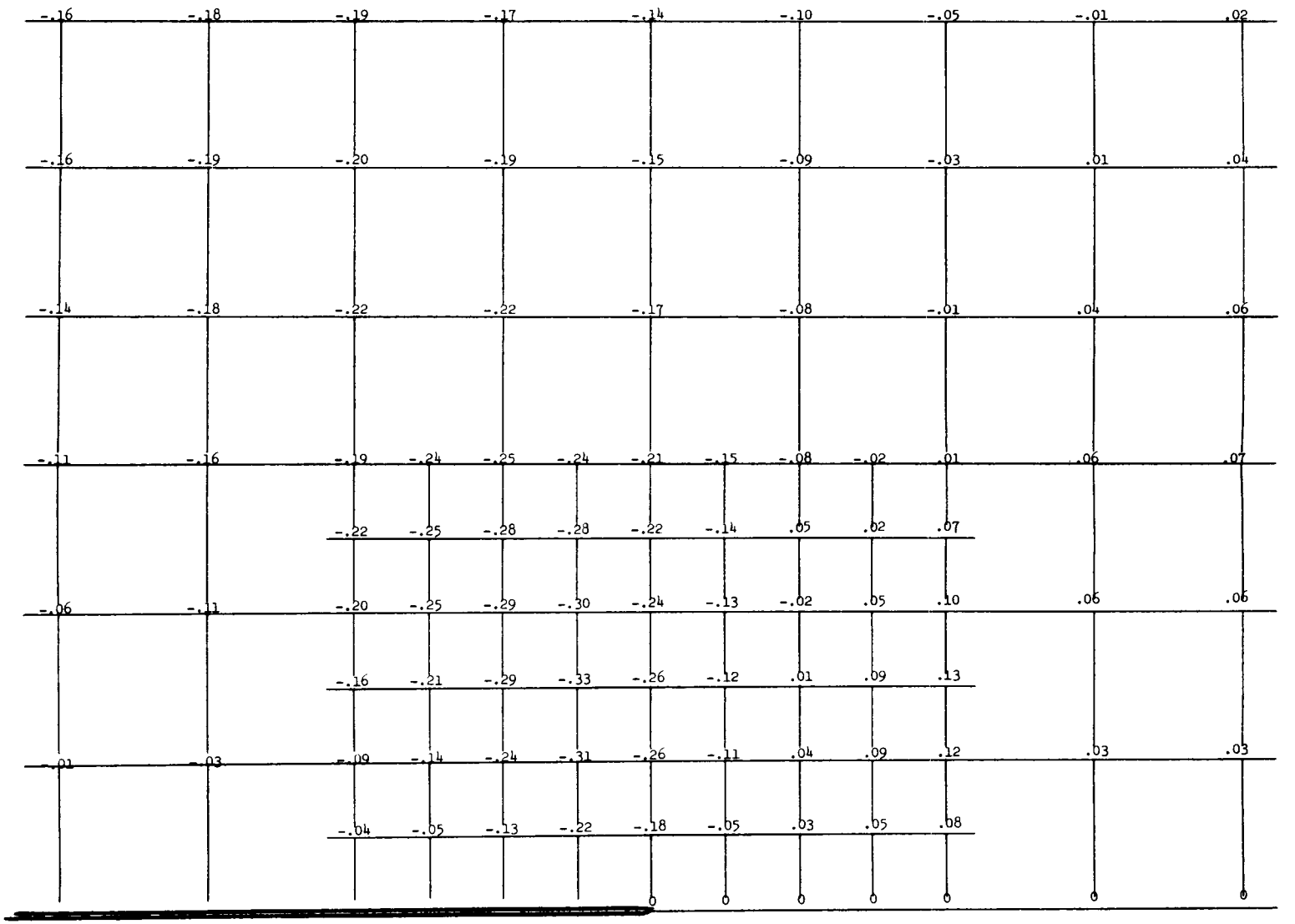

FIGURE 14. σ_{xy} DISTRIBUTION IN CRACKED PLATE SUBJECTED TO UNIFORM TENSION
ELASTIC-PLASTIC BOUNDARY AT $\underline{c}^2 = 4.17$
FINE GRID (GRID LENGTH h=1/2) ; COARSE GRID (h=1)

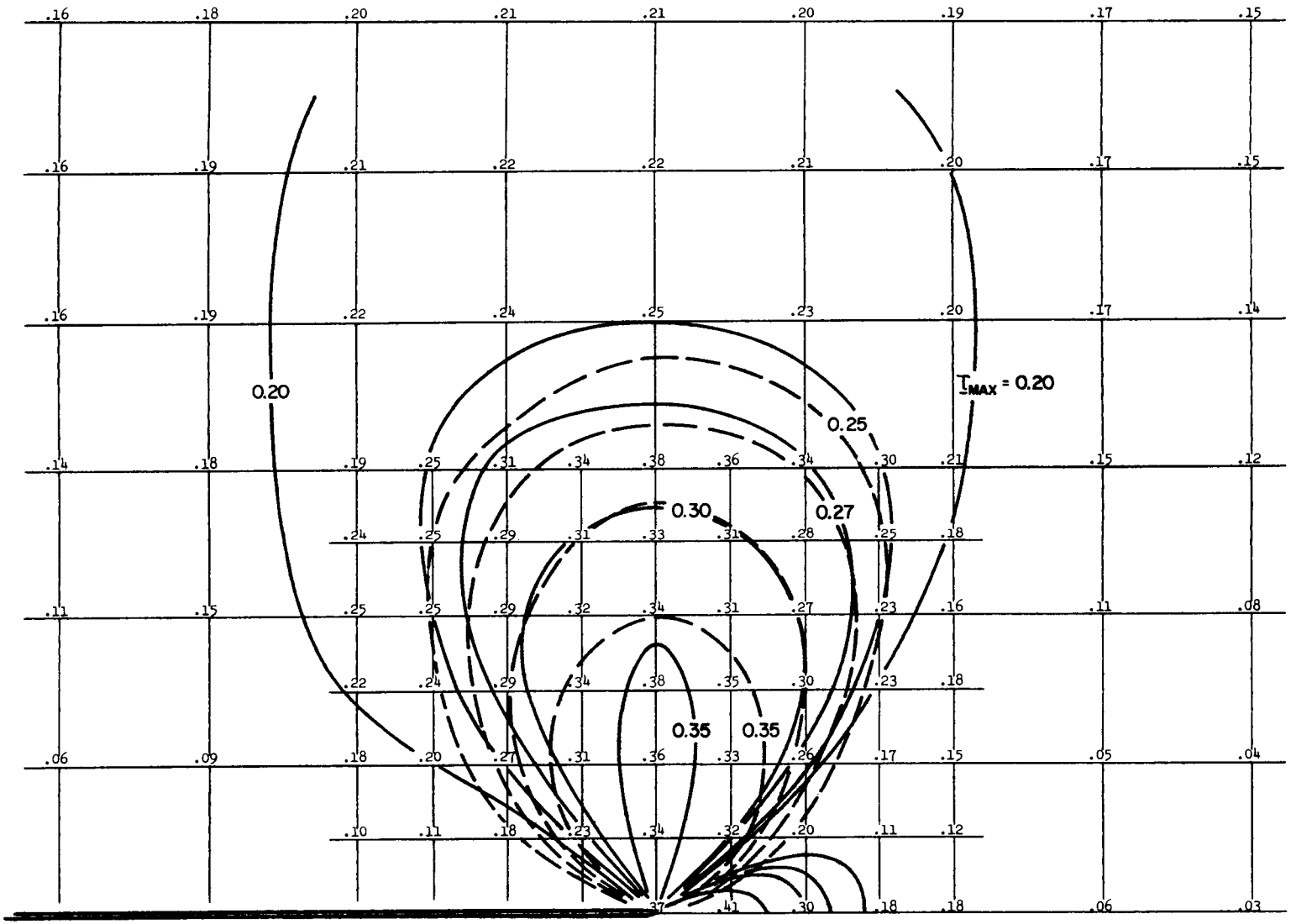

FIGURE 15. τ_{max} DISTRIBUTION IN CRACKED PLATE SUBJECTED TO UNIFORM TENSION

ELASTIC-PLASTIC BOUNDARY AT $c^2 = 4.17$

FINE GRID (GRID LENGTH h=1/2) ; COARSE GRID (h=1) ; SOLID LINES = ELASTIC-PLASTIC ANALYSIS ; DASHED LINES = ELASTIC ANALYSIS

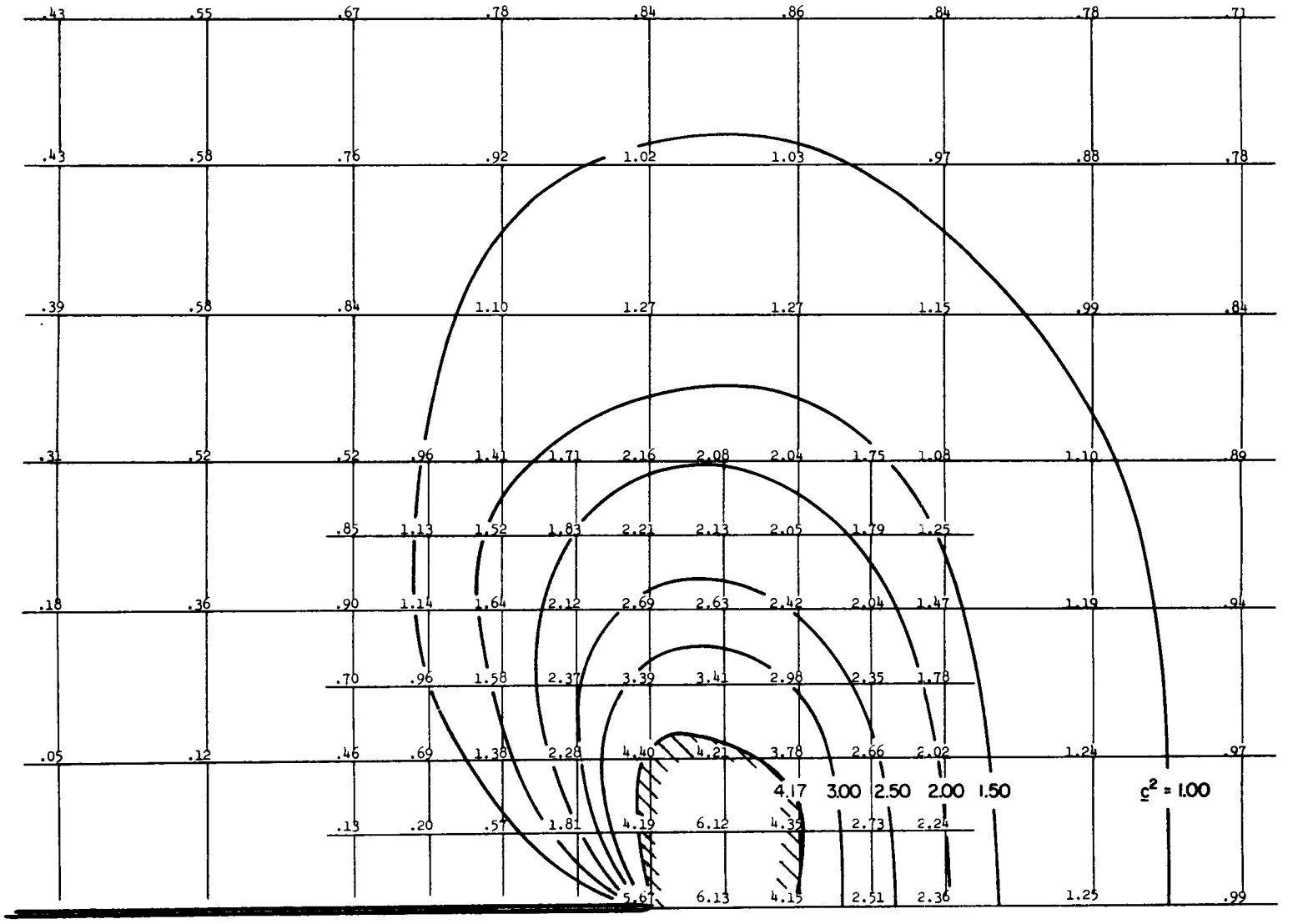

FIGURE 16. $\underline{c}^2$ DISTRIBUTION IN CRACKED PLATE SUBJECTED TO UNIFORM TENSION

ELASTIC-PLASTIC BOUNDARY AT $\underline{c}^2 = 4.17$

FINE GRID (GRID LENGTH h = 1/2) ; COARSE GRID (h = 1)

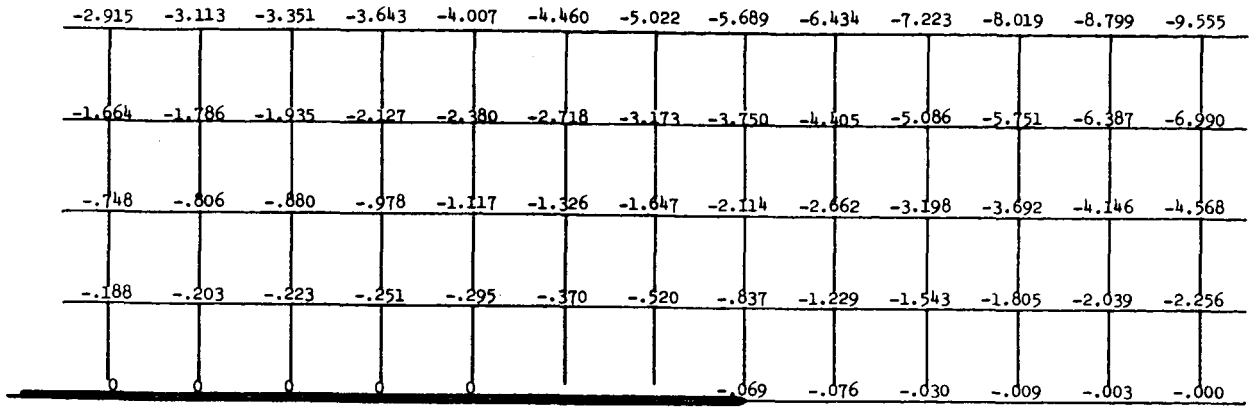

FIGURE 17. $\underline{X}_{11}$ DISTRIBUTION IN CRACKED PLATE SUBJECTED TO UNIFORM IN-PLANE SHEAR
ELASTIC-PLASTIC BOUNDARY AT $\underline{c}^2 = 1.57$
COARSE GRID (GRID LENGTH h = 1)

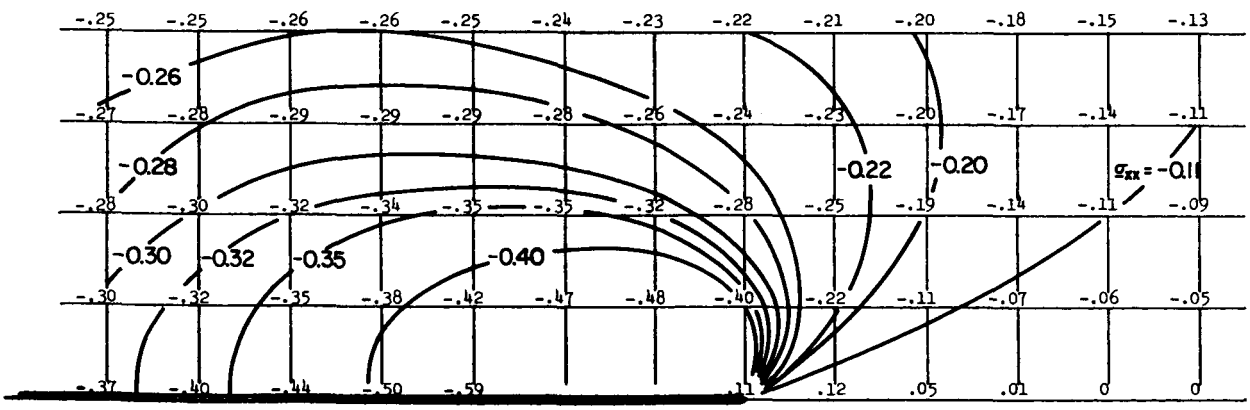

FIGURE 18. $\underline{\sigma}_{xx}$ DISTRIBUTION IN CRACKED PLATE SUBJECTED TO UNIFORM IN-PLANE SHEAR
ELASTIC-PLASTIC BOUNDARY AT $\underline{c}^2 = 1.57$
COARSE GRID (GRID LENGTH h = 1)

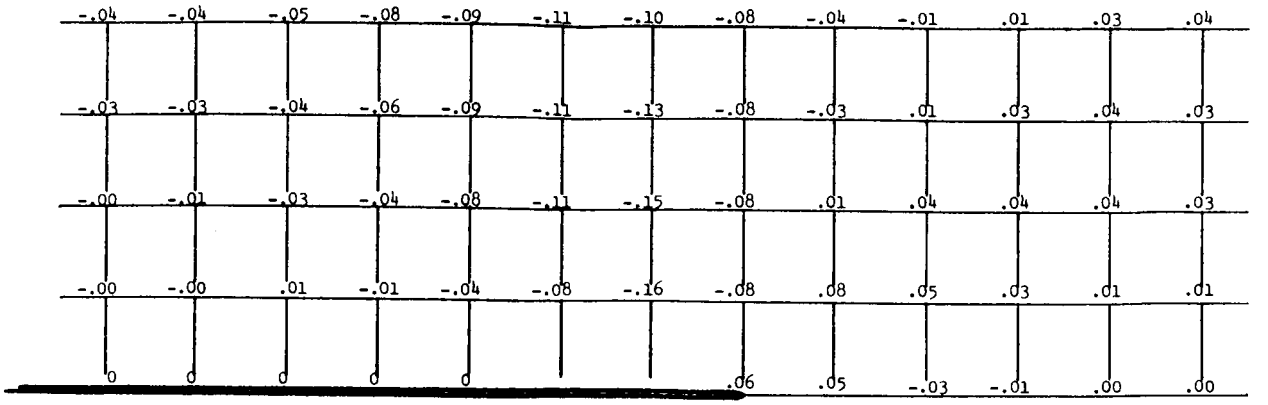

FIGURE 19. σ_{yy} DISTRIBUTION IN CRACKED PLATE SUBJECTED TO UNIFORM IN-PLANE SHEAR
ELASTIC-PLASTIC BOUNDARY AT $\zeta^2 = 1.57$
COARSE GRID (GRID LENGTH h = 1)

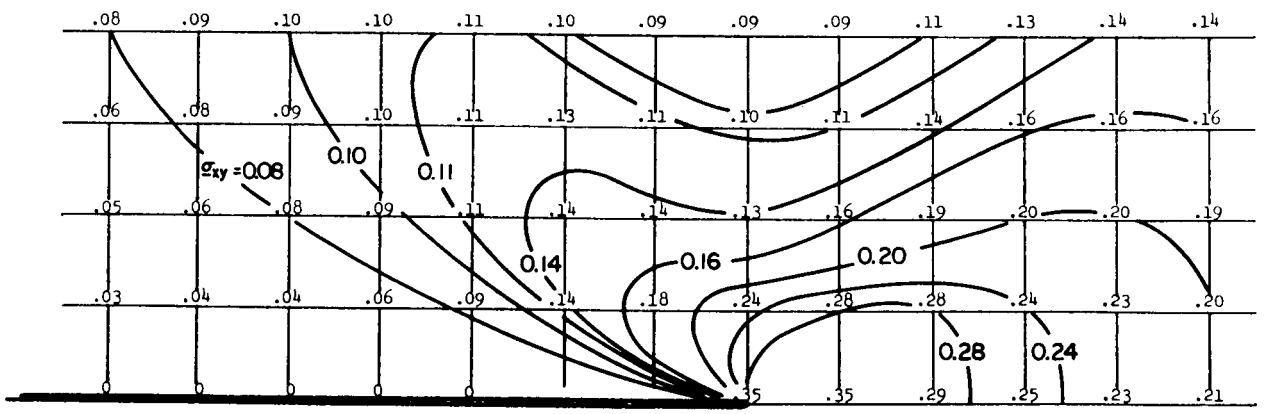

FIGURE 20. σ_{xy} DISTRIBUTION IN CRACKED PLATE SUBJECTED TO UNIFORM IN-PLANE SHEAR
ELASTIC-PLASTIC BOUNDARY AT $\zeta^2 = 1.57$
COARSE GRID (GRID LENGTH h = 1)

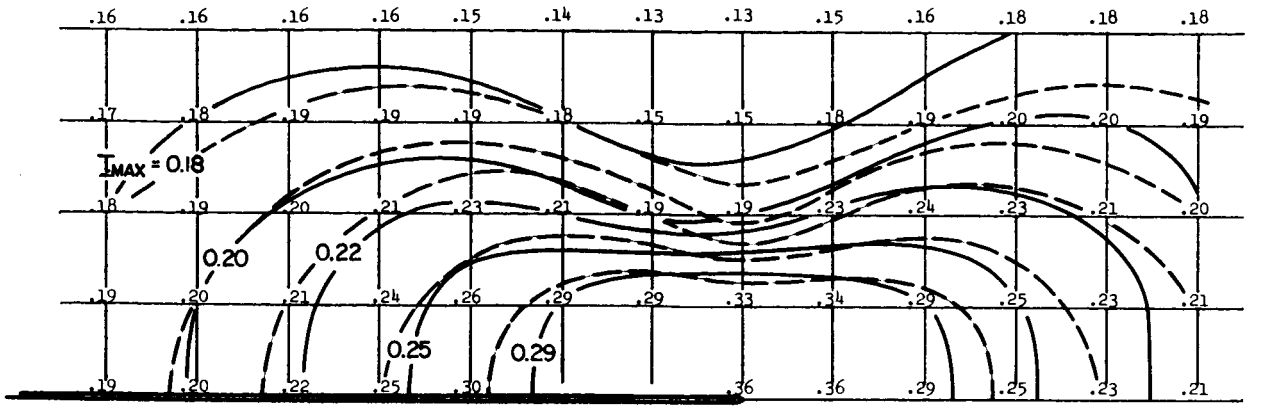

FIGURE 21. τ_{max} DISTRIBUTION IN CRACKED PLATE SUBJECTED TO UNIFORM IN-PLANE SHEAR
ELASTIC-PLASTIC BOUNDARY AT $\underline{c}^2 = 1.57$
COARSE GRID (GRID LENGTH h = 1) ; SOLID LINES = ELASTIC-PLASTIC ANALYSIS ; DASHED LINES = ELASTIC ANALYSIS

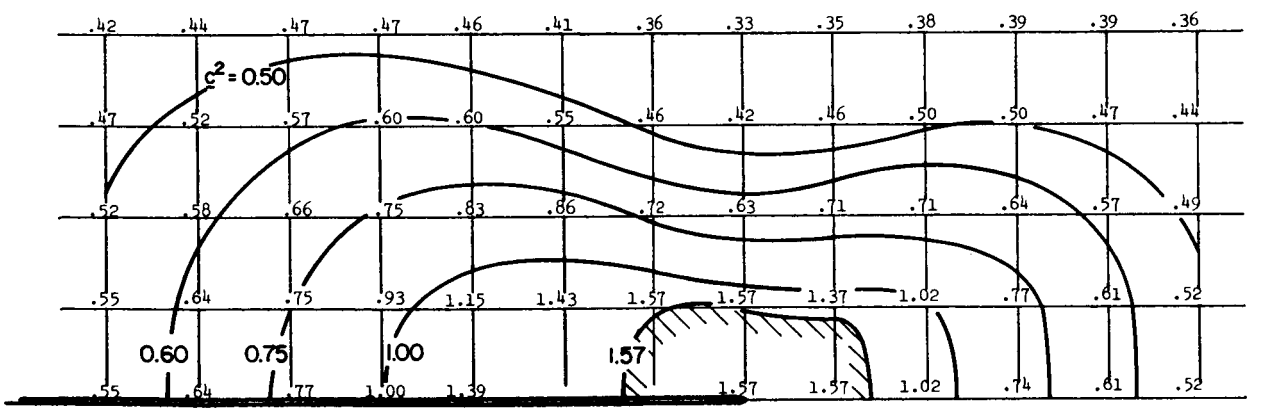

FIGURE 22. $\underline{c}^2$ DISTRIBUTION IN CRACKED PLATE SUBJECTED TO UNIFORM IN-PLANE SHEAR
ELASTIC-PLASTIC BOUNDARY AT $\underline{c}^2 = 1.57$
COARSE GRID (GRID LENGTH h = 1)

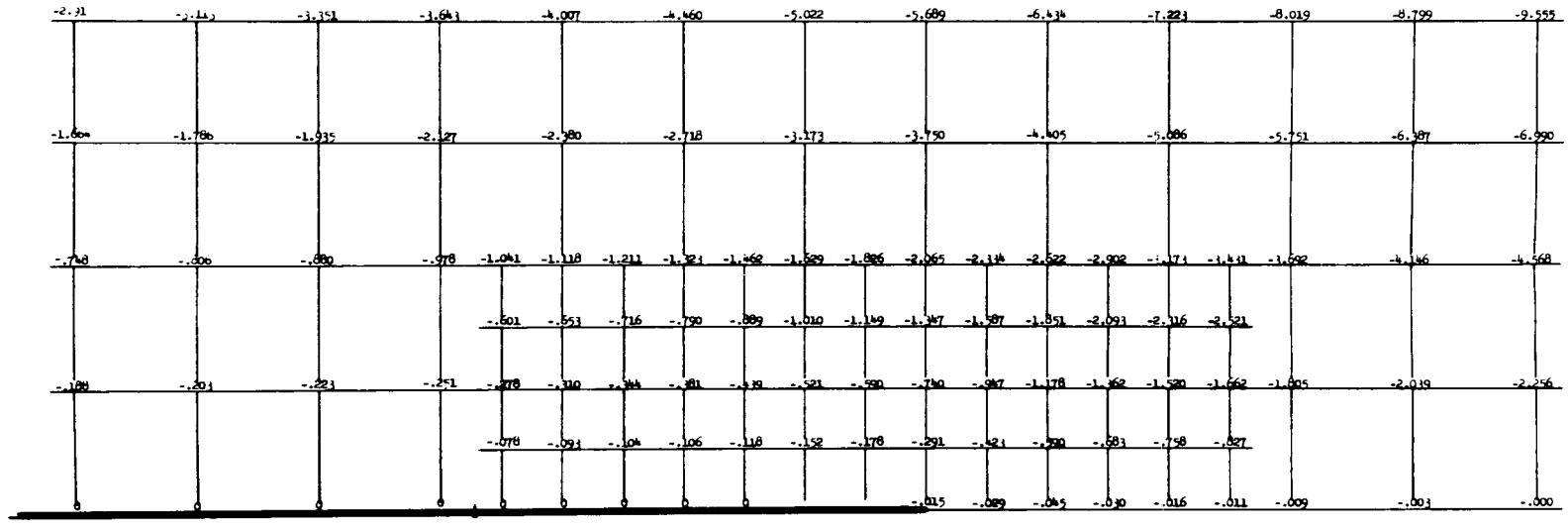

FIGURE 23. $\underline{\kappa}_{11}$ DISTRIBUTION IN CRACKED PLATE SUBJECTED TO UNIFORM IN-PLANE SHEAR

ELASTIC-PLASTIC BOUNDARY AT $\xi^2 = 2.87$

FINE GRID (GRID LENGTH h=1/2) ; COARSE GRID (h=1)

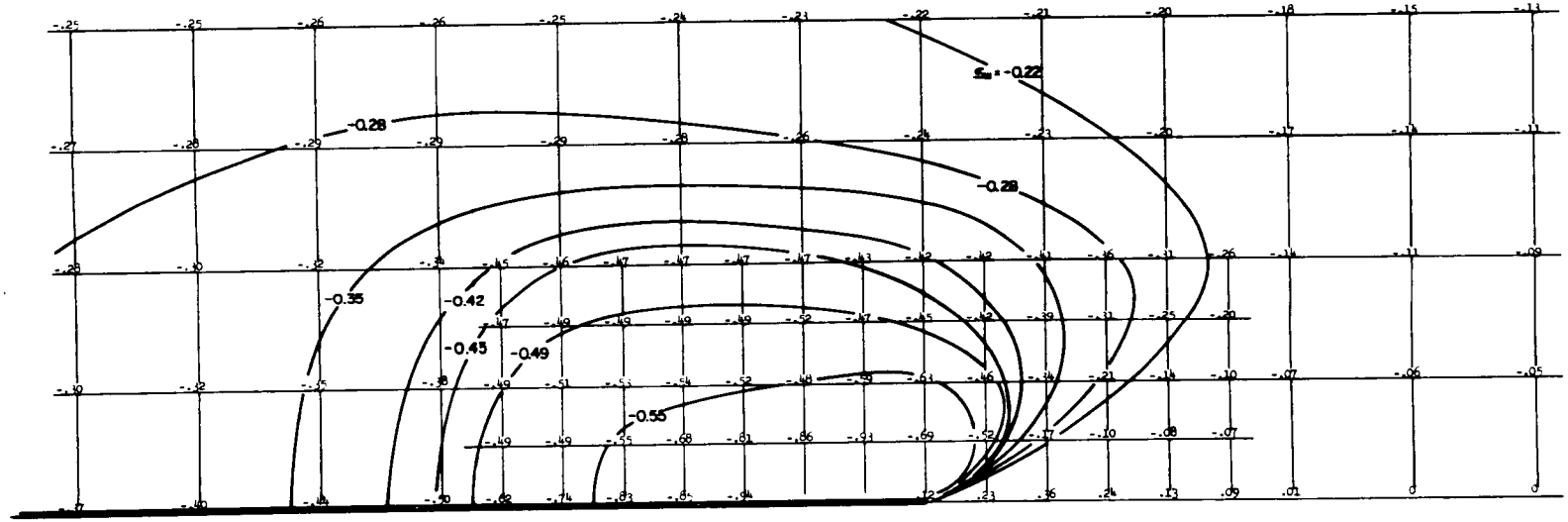

FIGURE 24. σ_{xx} DISTRIBUTION IN CRACKED PLATE SUBJECTED TO UNIFORM IN-PLANE SHEAR

ELASTIC-PLASTIC BOUNDARY AT $\xi^2 = 2.87$

FINE GRID (GRID LENGTH h = 1/2) ; COARSE GRID (h = 1)

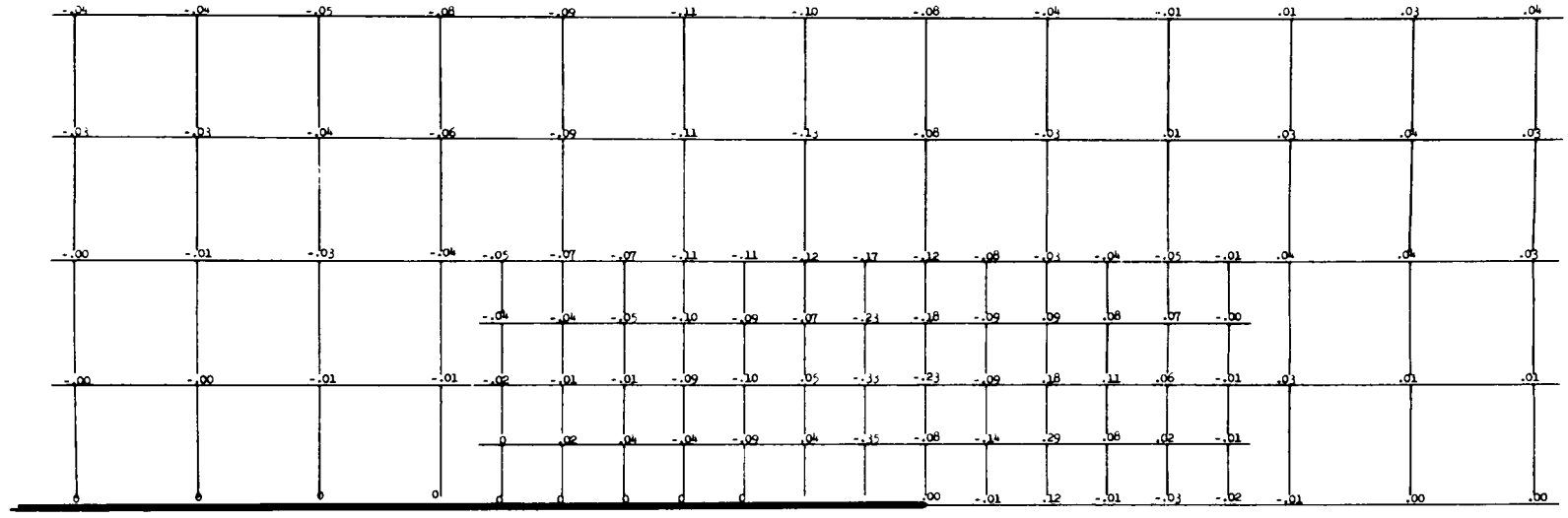

FIGURE 25. σ_{yy} DISTRIBUTION IN CRACKED PLATE SUBJECTED TO UNIFORM IN-PLANE SHEAR

ELASTIC-PLASTIC BOUNDARY AT $\xi^2 = 2.87$

FINE GRID (GRID LENGTH $h = 1/2$) , COARSE GRID ($h = 1$)

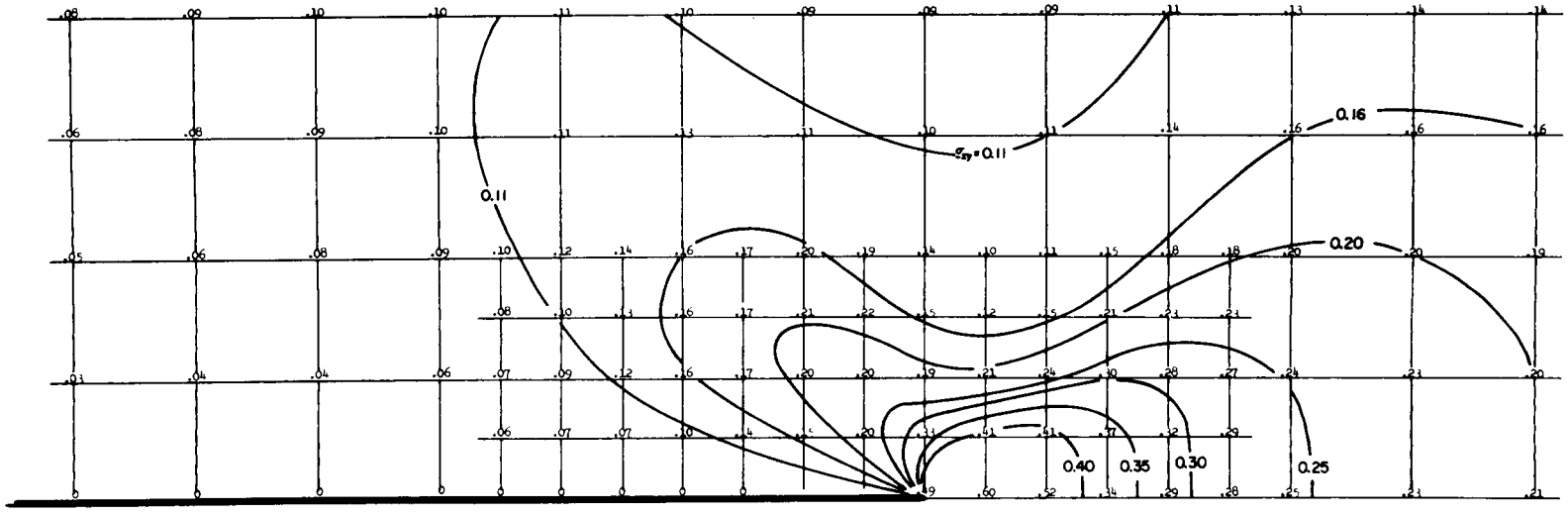

FIGURE 26. σ_{xy} DISTRIBUTION IN CRACKED PLATE SUBJECTED TO UNIFORM IN-PLANE SHEAR

ELASTIC-PLASTIC BOUNDARY AT $\xi^2 = 2.87$

FINE GRID (GRID LENGTH h=1/2) ; COARSE GRID (h=1)

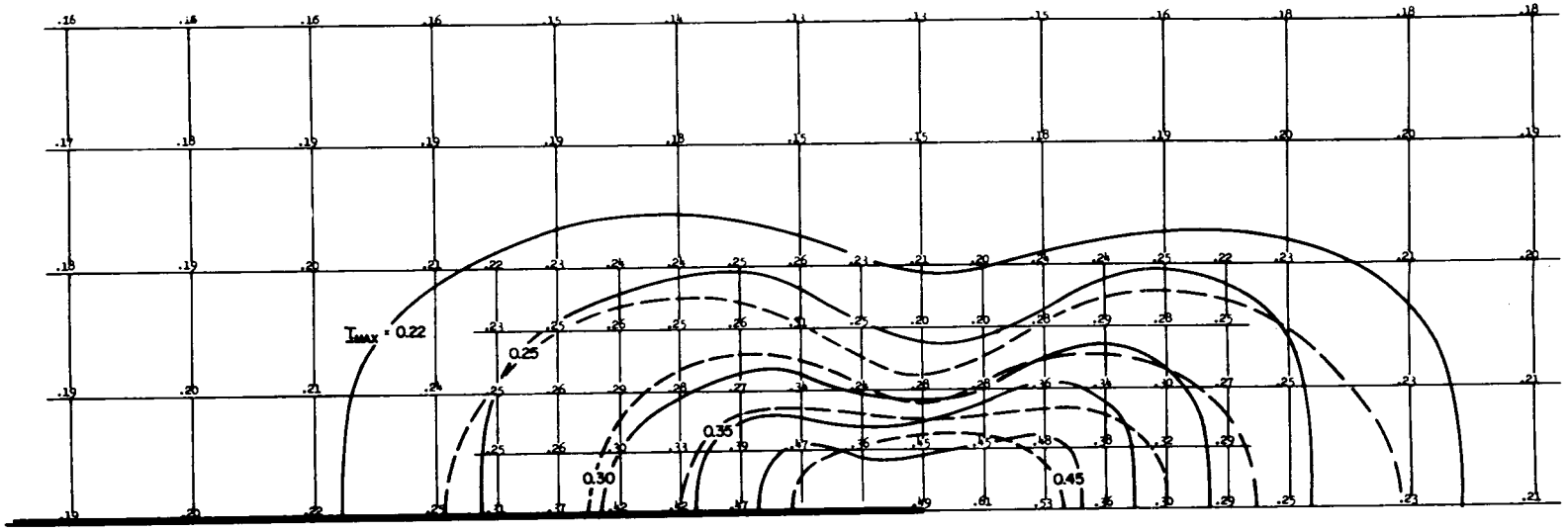

FIGURE 27. τ_{max} DISTRIBUTION IN CRACKED PLATE SUBJECTED TO UNIFORM IN-PLANE SHEAR

ELASTIC-PLASTIC BOUNDARY AT $\xi^2 = 2.87$

FINE GRID (GRID LENGTH h=1/2) ; COARSE GRID (h=1) ; SOLID LINES = ELASTIC-PLASTIC ANALYSIS ; DASHED LINES = ELASTIC ANALYSIS

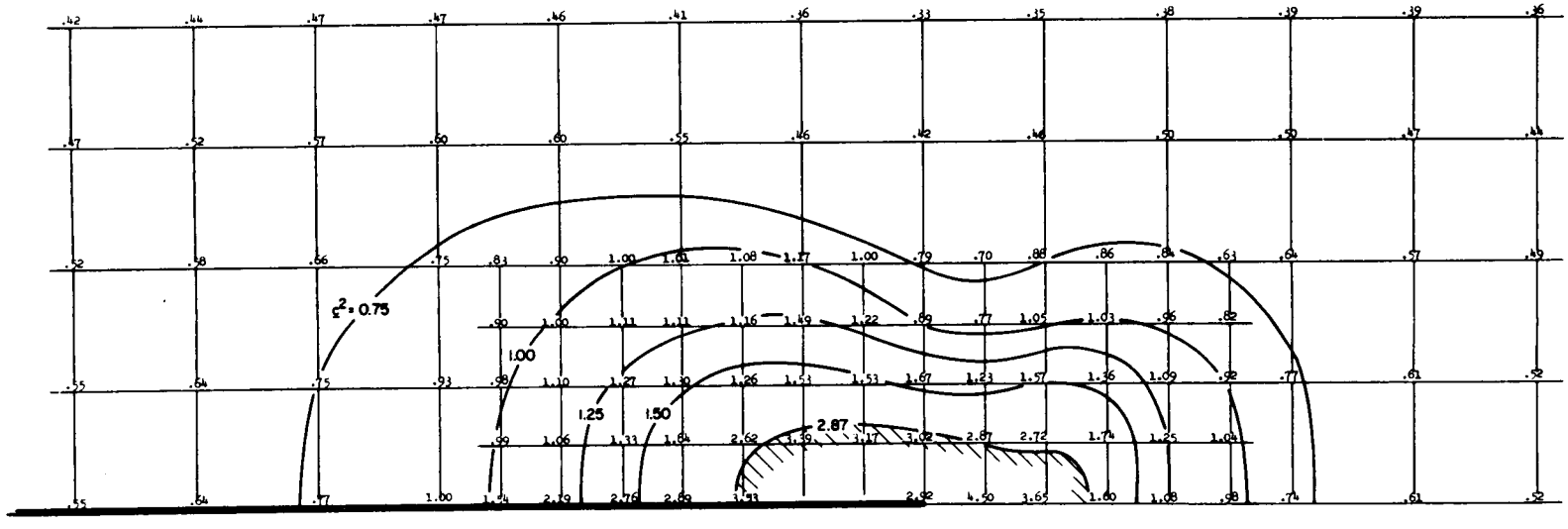

FIGURE 28. ξ^2 DISTRIBUTION IN CRACKED PLATE SUBJECTED TO UNIFORM IN-PLANE SHEAR

ELASTIC-PLASTIC BOUNDARY AT $\xi^2 = 2.87$

FINE GRID (GRID LENGTH h = 1/2) ; COARSE GRID (h = 1)

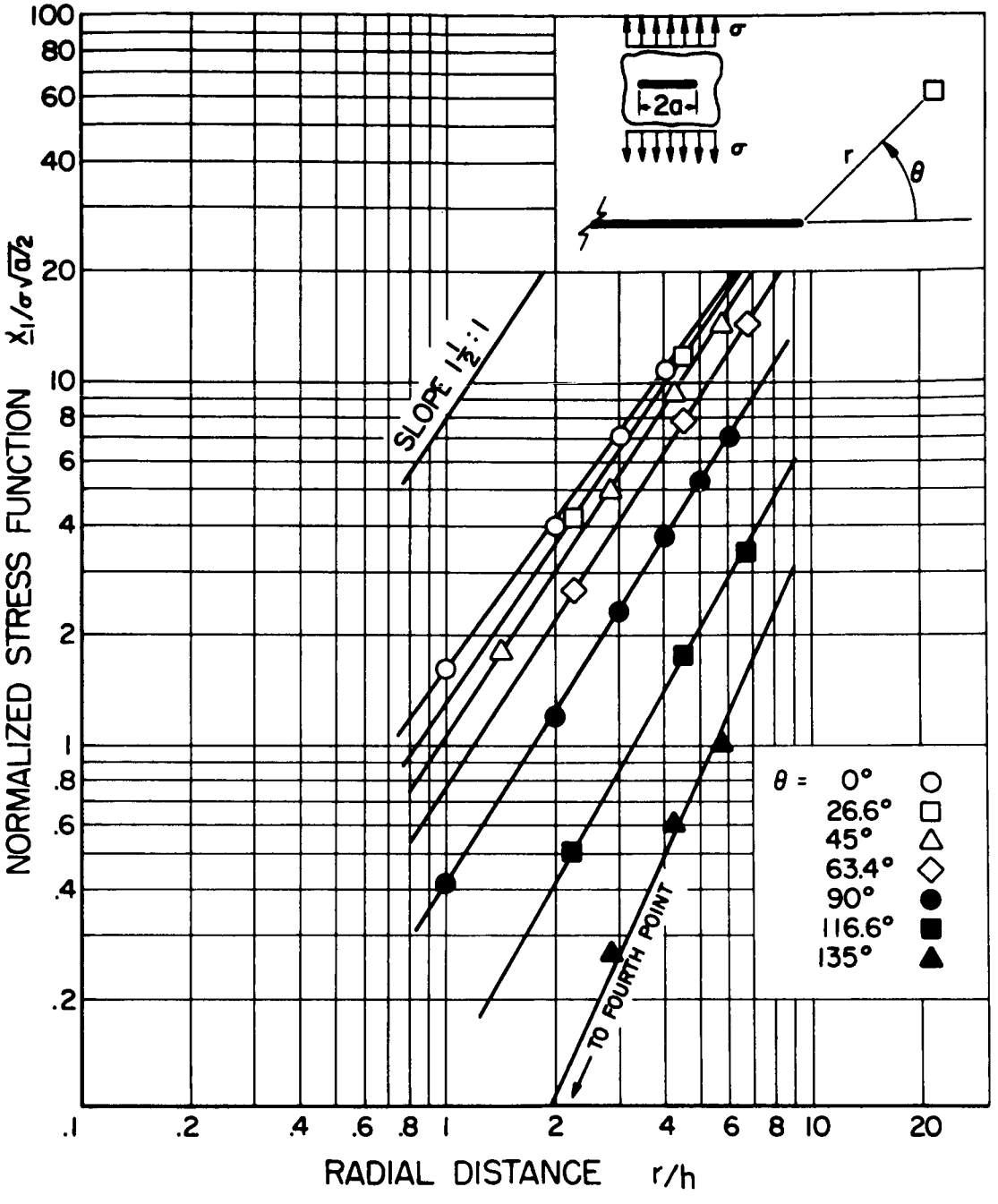

FIGURE 29. STRESS FUNCTIONS (χ_1) vs RADIAL DISTANCES (r/h WHERE h=1)

COARSE GRID, $\xi^2 = 3.25$

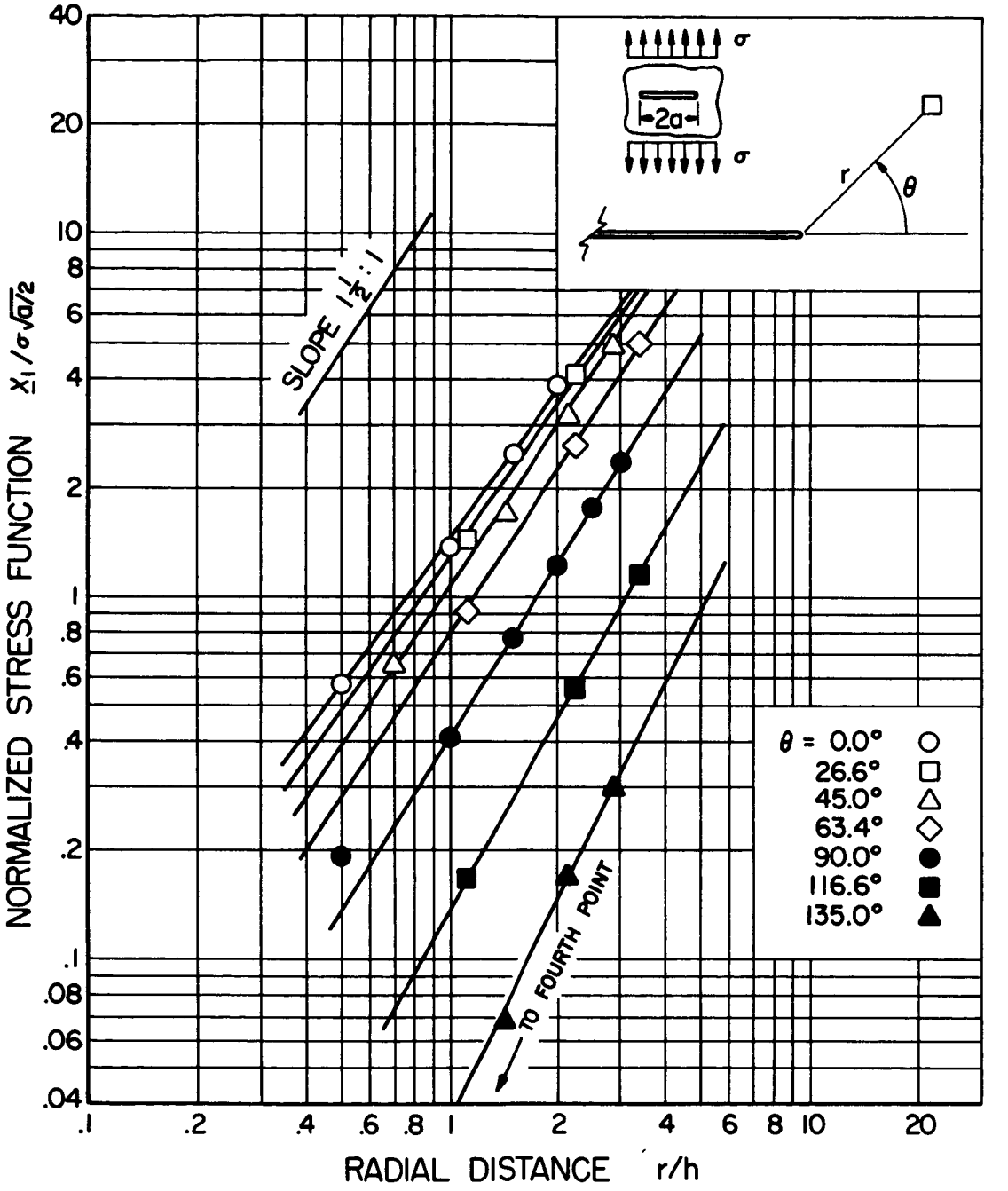

FIGURE 30. STRESS FUNCTIONS ($\underline{X}_1$) vs RADIAL DISTANCES (r/h WHERE h = 1)

FINE GRID , $\underline{c}^2 = 4.17$

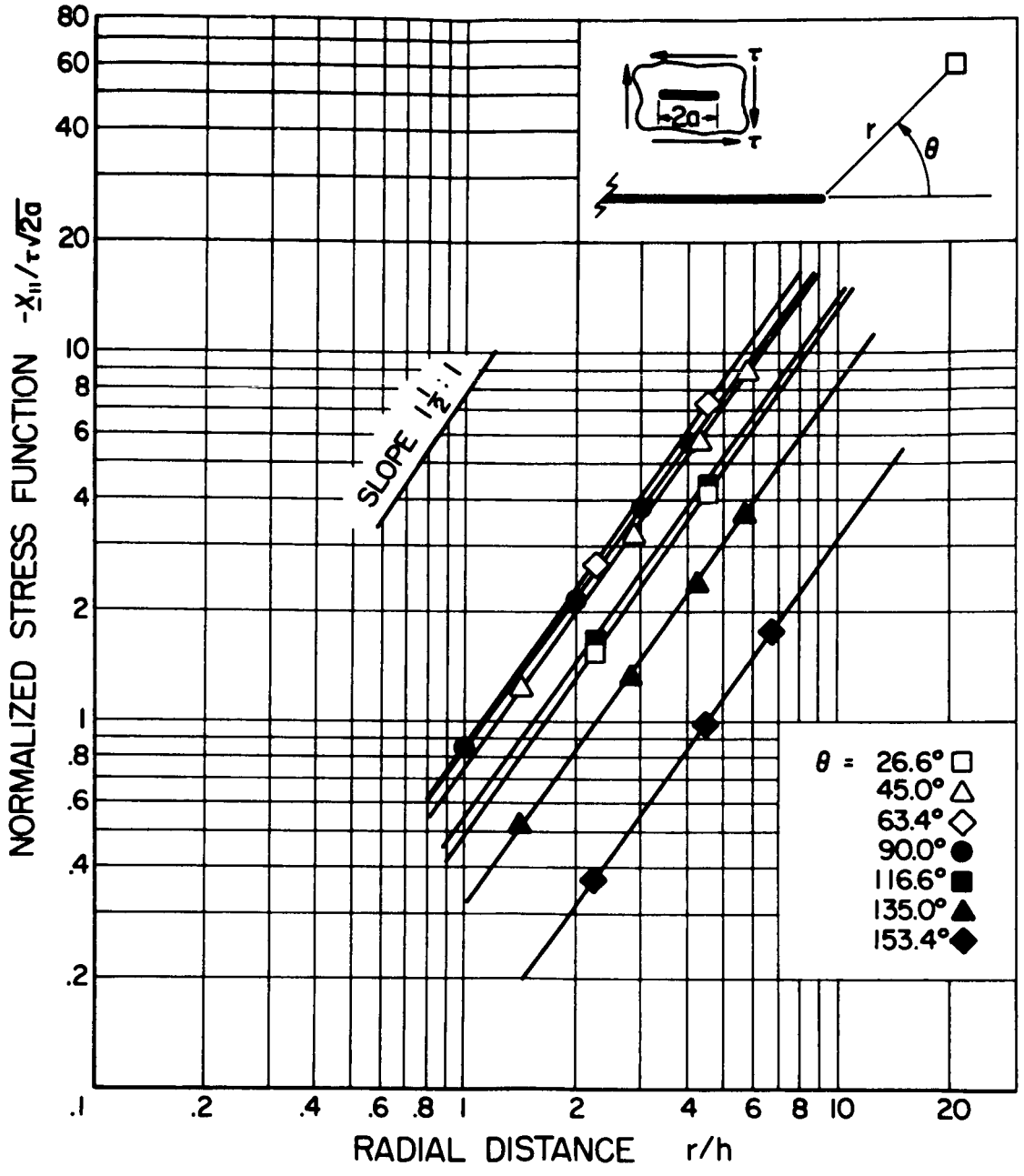

FIGURE 31. STRESS FUNCTIONS (χ_{11}) vs RADIAL DISTANCES (r/h WHERE h=1)

COARSE GRID, $c^2 = 1.57$

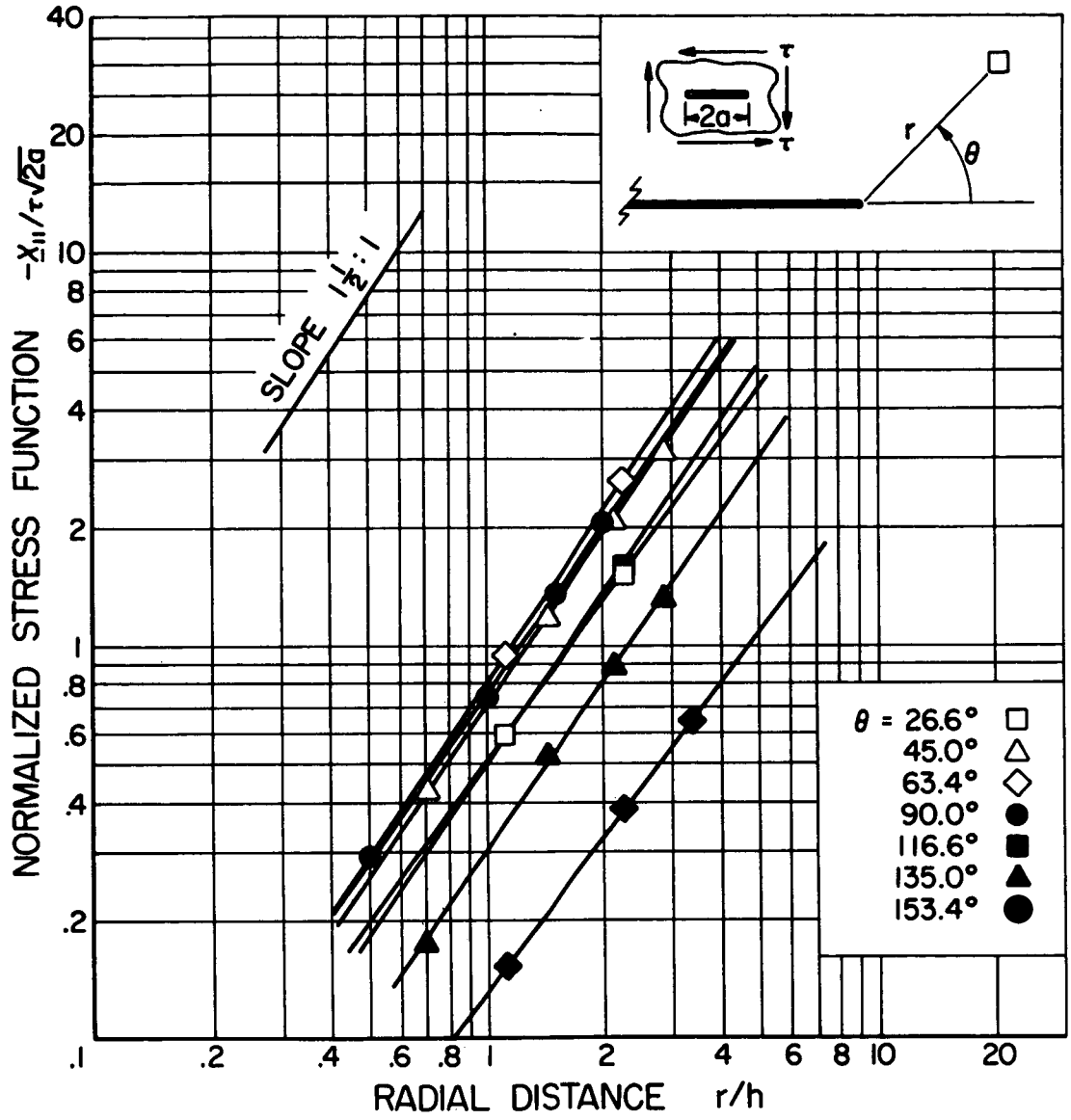

FIGURE 32. STRESS FUNCTIONS ($\underline{X}_{11}$) vs RADIAL DISTANCES (r/h WHERE h=1)

FINE GRID , $\underline{c}^2 = 2.87$

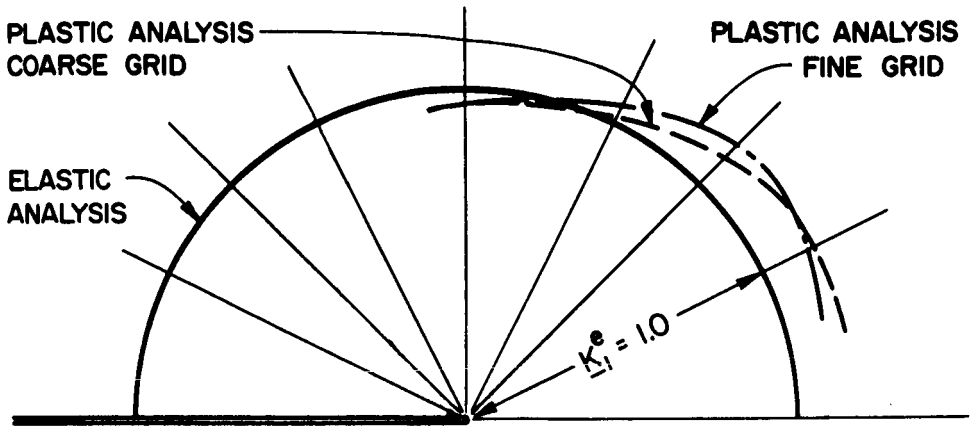

FIGURE 33. VALUES OF K_I AT VARIOUS ANGLES.

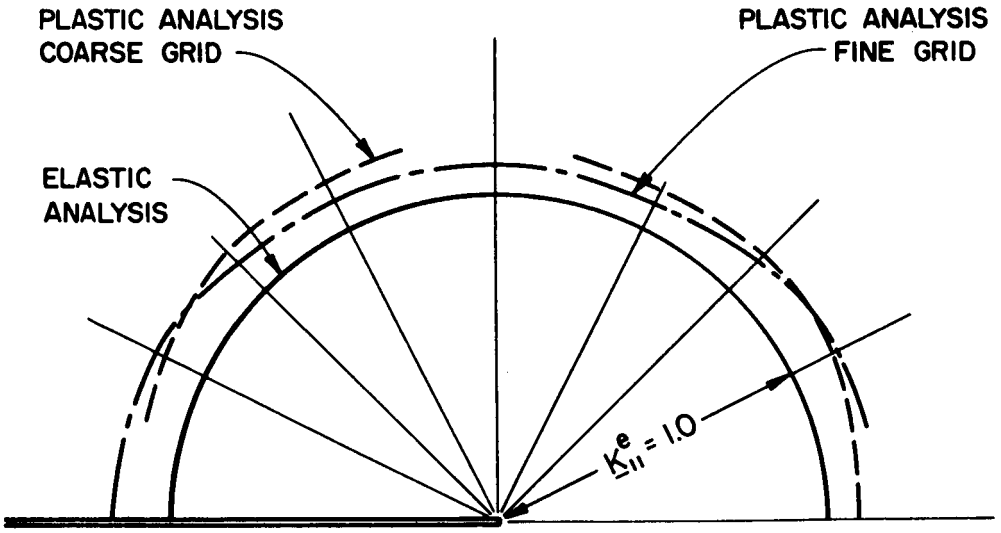

FIGURE 34. VALUES OF K_{II} AT VARIOUS ANGLES.

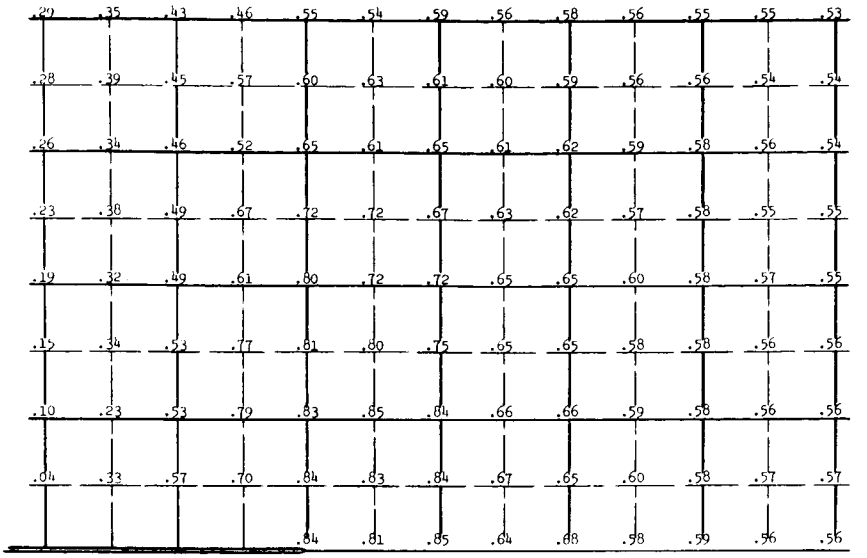

FIGURE 35. σ_{yy} DISTRIBUTION IN CRACKED PLATE SUBJECTED TO UNIFORM TENSION
ELASTIC-PLASTIC BOUNDARY AT $\zeta^2 = 2.15$
SOLID LINES = ORIGINAL GRID ; DASHED LINES = SHIFTED GRID

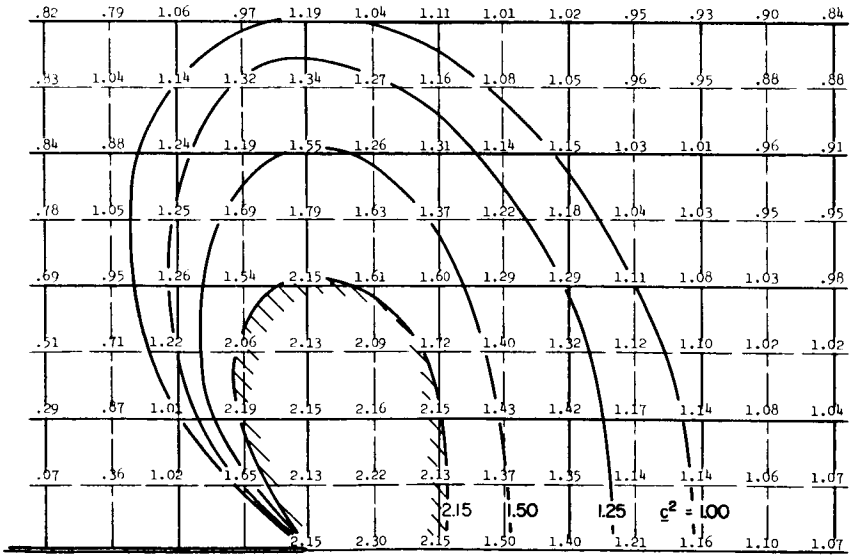

FIGURE 36. ζ^2 DISTRIBUTION IN CRACKED PLATE SUBJECTED TO UNIFORM TENSION
ELASTIC-PLASTIC BOUNDARY AT $\zeta^2 = 2.15$
SOLID LINES = ORIGINAL GRID ; DASHED LINES = SHIFTED GRID

"The aeronautical and space activities of the United States shall be conducted so as to contribute . . . to the expansion of human knowledge of phenomena in the atmosphere and space. The Administration shall provide for the widest practicable and appropriate dissemination of information concerning its activities and the results thereof."

—NATIONAL AERONAUTICS AND SPACE ACT OF 1958

NASA SCIENTIFIC AND TECHNICAL PUBLICATIONS

TECHNICAL REPORTS: Scientific and technical information considered important, complete, and a lasting contribution to existing knowledge.

TECHNICAL NOTES: Information less broad in scope but nevertheless of importance as a contribution to existing knowledge.

TECHNICAL MEMORANDUMS: Information receiving limited distribution because of preliminary data, security classification, or other reasons.

CONTRACTOR REPORTS: Scientific and technical information generated under a NASA contract or grant and considered an important contribution to existing knowledge.

TECHNICAL TRANSLATIONS: Information published in a foreign language considered to merit NASA distribution in English.

SPECIAL PUBLICATIONS: Information derived from or of value to NASA activities. Publications include conference proceedings, monographs, data compilations, handbooks, sourcebooks, and special bibliographies.

TECHNOLOGY UTILIZATION PUBLICATIONS: Information on technology used by NASA that may be of particular interest in commercial and other non-aerospace applications. Publications include Tech Briefs, Technology Utilization Reports and Notes, and Technology Surveys.

Details on the availability of these publications may be obtained from:

SCIENTIFIC AND TECHNICAL INFORMATION DIVISION

NATIONAL AERONAUTICS AND SPACE ADMINISTRATION

Washington, D.C. 20546